Transworld Research Network
37/661 (2), Fort P.O., Trivandrum-695 023, Kerala, India

Functional and Structural Biology on the Lipo-network, 2006: 135-164
ISBN: 81-7895-232-7 Editors: Kosuke Morikawa and Shin-ichi Tate

8

Biochemical and structural characteristics of hematopoietic prostaglandin D synthase: From evolutionary analysis to drug designing

Yoshihiro Urade[1], Ikuko Mohri[1], Kosuke Aritake[1], Tsuyoshi Inoue[2] and Masashi Miyano[3]
[1]Department of Molecular Behavioral Biology, Osaka Bioscience Institute Osaka 565-0874, Japan; [2]Department of Applied Chemistry, Graduate School of Engineering, Osaka University, Osaka 565-0871, Japan
[3]Structural Biophysics Laboratory, RIKEN SPring-8 Center Harima Institute, Hyogo 679-5148, Japan

Abstract

Hematopoietic prostaglandin (PG) D sythase (H-PGDS) catalyzes the isomerization of PGH_2, a common intermediate of various prostanoids, to PGD_2, an inflammatory mediator, in the presence of glutathione (GSH). H-PGDS is activated by Mg^{2+}, which increases the affinity of the enzyme for GSH and the turnover number. An evolutionary study revealed H-PGDS to be

Correspondence/Reprint request: Dr. Yoshihiro Urade, Department of Molecular Behavioral Biology, Osaka Bioscience Institute, Osaka 565-0874, Japan. E-mail: uradey@obi.or.jp

the first identified mammalian member of the sigma class of GSH-transferases. The crystallographic analysis of the rat and human enzymes identified a prominent cleft near the bound GSH to be the catalytic center. In the human enzyme, the Mg^{2+} ion is octahedrally coordinated by 6 water molecules at the interface of a homodimer, in which Asp93, Asp96, and Asp97 from each subunit surround 6 water molecules. An orally effective H-PGDS inhibitor, 4-benzhydryloxy-1-[3-(1H-tetrazol-5-yl)-propyl]-piperidine (HQL-79) was found to bind within the catalytic cleft between Trp104 and GSH. Oral administration of HQL-79 suppressed antigen-induced eosinophilic accumulation in the lung of wild-type mice and human H-PGDS-overexpressing mice, gliosis and demyelination in twitcher mice, and muscular distrophy in mdx mice. The tertiary structure of H-PGDS gives informative clues for the development of inhibitors specific for this enzyme, of which inhibitors are promising drugs to suppress allergic inflammation, neuroinflammation, and muscular dystrophy.

Introduction

Prostaglandin (PG) D_2 is a mediator of allergic and inflammatory responses produced by mast cells (1) and Th2 cells (2) in a variety of tissues, and is also an endogenous somnogen acting within the brain (3). PGD_2 is formed from arachidonic acid by successive enzyme reactions (**Fig. 1**): PG endoperoxide synthase (cyclooxygenase, COX) catalyzes the di-oxygenation of arachidonic acid to PGH_2 *via* PGG_2, and PGD synthase (PGDS) then catalyzes the isomerization of PGH_2 to PGD_2 (3). There are 2 distinct types of PGDS: one is hematopoietic PGDS (H-PGDS) localized in mast cells (1), Th2 cells (2) and microglia (4); and the other is lipocalin-type PGDS (L-PGDS) localized in leptomeninges, choroids plexus, and oligodendrocytes in the brain (5,6).

Asthmatic responses are attenuated in mice whose gene for the DP (DP_1) receptor specific for PGD_2 has been knocked out (7). The DP_1 receptor is constitutively expressed in human basophils and eosinophils and is induced in pulmonary and airway epithelial cells by allergens and inflammation (7). PGD_2 also acts as a ligand for an orphan receptor, CRTH2 (DP_2), which is expressed in human Th2 cells, eosinophils, and basophils, and mediates the chemotaxis of these cells toward PGD_2 (8,9). Molecular and pharmacological properties of DP_1 and DP_2 receptors are summarized in **Table 1**. In contrast, overproduction of PGD_2 exacerbates asthmatic responses, as demonstrated in ovalbumin-challenged mice transgenic for human L-PGDS (10).

PGD_2 is further converted to 9α,11β-PGF_2, a stereoisomer of $PGF_{2\alpha}$, which exerts various pharmacological actions different from those induced by $PGF_{2\alpha}$ (reviewed by Smith et al. (11)). PGD_2 is also readily dehydrated *in vitro* (12) to produce PGs of the J series, such as PGJ_2, Δ^{12}-PGJ_2, and 15-deoxy-$\Delta^{12,14}$-PGJ_2.

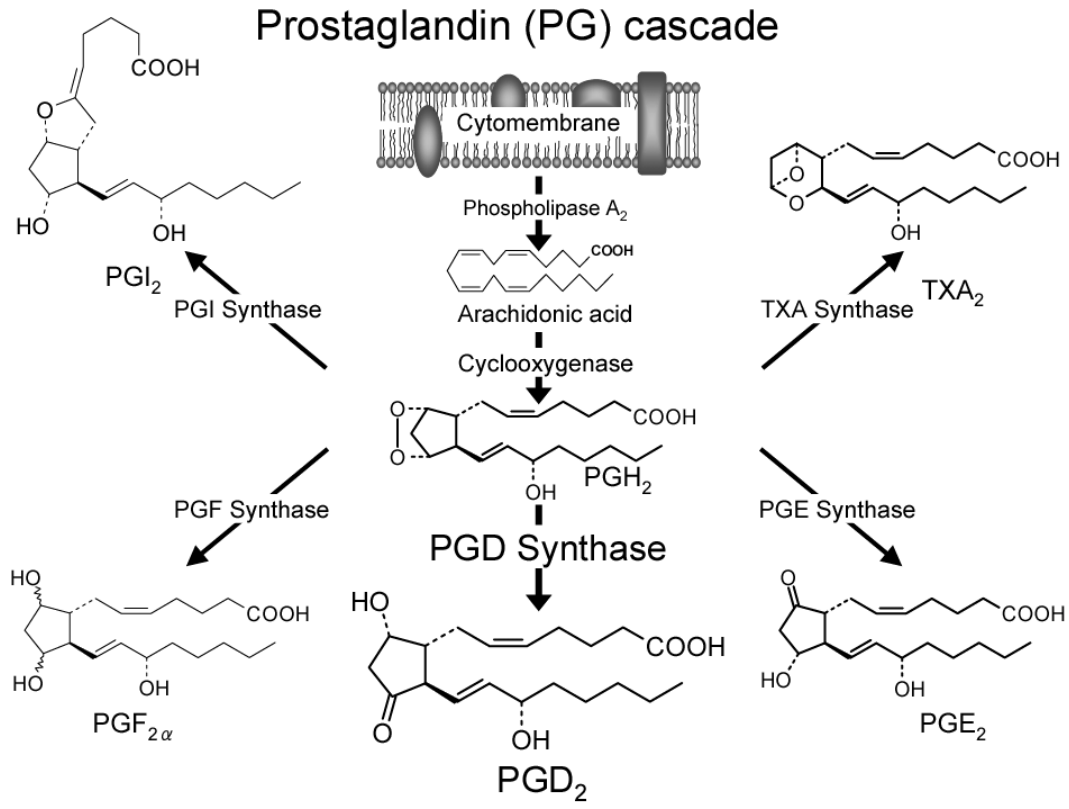

Figure 1. Prostanoid cascade.

Table 1. Biochemical and pharmacological properties of DP_1 and DP_2 receptors.

Subtype	DP_1 (DP)	DP_2 (CRTH2)
Second messenger	Gs type (cAMP ↑)	Gi/o type (cAMP ↓, Ca^{2+} ↑)
Distribution (Function)	Platelet (aggregation) Trachea (contraction) CNS (sleep) Astrocytes (activation)	Th2 cells (chemotaxis) Eosinophils/Basophils Astrocytes (activation)
Agonist	BW 245C	13,14-dihydro-15-keto prostaglandin D_2
Antagonist	BW A868C, S-5751	Ramatroban

15-Deoxy-$\Delta^{12,14}$-PGJ_2 acts as a ligand for a nuclear receptor, peroxisome proliferator-activated receptor γ (PPARγ), and promotes adipocyte differentiation (13,14). Although the production and occurrence of the J series of PGs *in vivo* have long been proposed by several research groups (15), such a proposition is now extremely questionable, because we and other groups have never detected the J series of PGs in fresh tissue samples or body fluids (16,17).

Biochemical properties

1) Enzymatic properties of H-PGDS

H-PGDS was originally purified in 1979 from rat spleen by Christ-Hazelhof and Nugteren as a cytosolic monomeric glutathione (GSH)-requiring PG endoperoxide D-isomerase (EC 5.3.99.2, **Fig. 2**) with a M_r of 26,000 (18). Since the M_r of H-PGDS was the same as that of L-PGDS (19-21), which had previously been miss-identified as a protein with a M_r of 80,000 (22), we re-examined the biochemical characteristics of H-PGDS and confirmed that H-PGDS was quite distinct from L-PGDS in terms of kinetic parameters, amino acid composition, and immunological properties (23). During the re-examination study, we found that H-PGDS was associated with the activity of GSH S-transferase (GST).

Although both H-PGDS and L-PGDS catalyze the same reaction, these enzymes have evolved from their ancestral origins differently from each other, H-PGDS from GST (as described later) and L-PGDS from lipocalins, which bind and transport various lipophilic substances (20,21,24). Therefore, we proposed that H-PGDS and L-PGDS are novel examples of functional convergence (3,25).

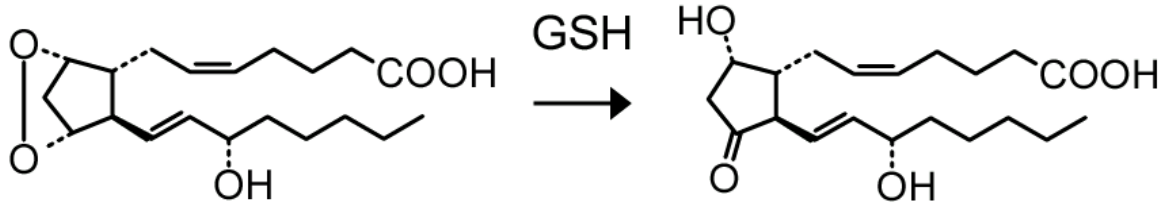

Figure 2. Enzymatic reaction of PGH_2 D-isomerase.

2) Activation of human H-PGDS by Mg^{2+}

We recently found that Ca^{2+} and Mg^{2+} ions increased the activity of H-PGDS to ~150% of its basal level in a concentration-dependent manner (**Fig. 3**), with half-maximum effective concentrations of 400 μM for Ca^{2+} and 50 μM for Mg^{2+} (26). Ca^{2+} did not change the affinity of human H-PGDS for GSH (K_m = 0.60 and 0.59 mM in the absence or presence, respectively, of 2 mM $CaCl_2$); whereas Mg^{2+} increased the affinity for GSH, decreasing the K_m value 4-fold to 0.14 mM. Although at the highest soluble concentration of PGH_2 (0.4 mM) the PGDS activity was not saturated, the calculated K_m value for PGH_2 changed slightly, from 0.46 mM in the absence of Ca^{2+} or Mg^{2+} to 0.33 or 0.93 mM in the presence of 2 mM $CaCl_2$ or $MgCl_2$, respectively. H-PGDS is localized in the cytosol, where the concentration of Mg^{2+} is estimated to be on the order of several mM. Thus, H-PGDS likely exists as the Mg^{2+}-bound form *in vivo*.

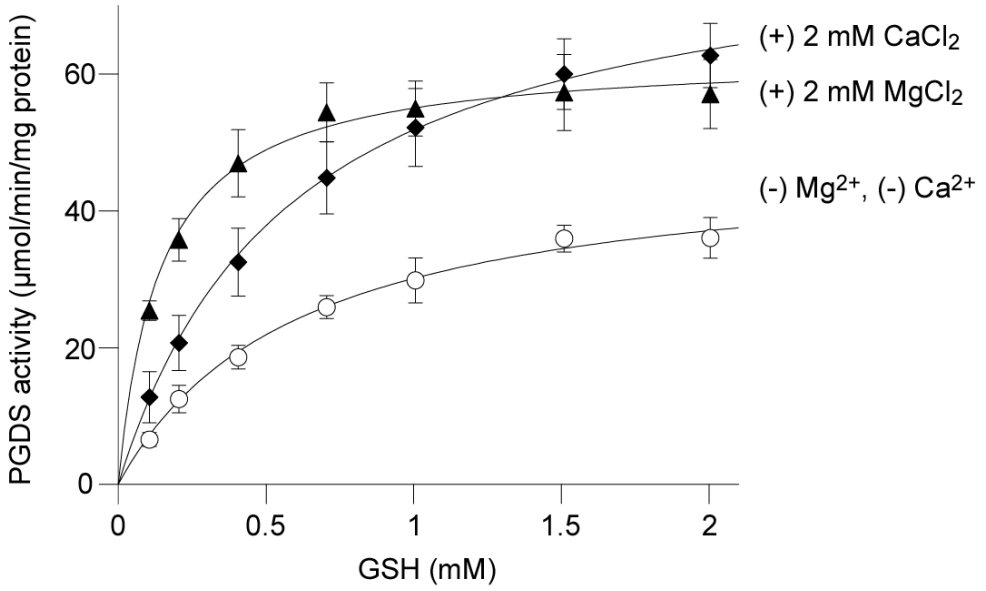

Figure 3. Activation of human H-PGDS by Mg^{2+} and Ca^{2+} (26).

3) Homodimer of H-PGDS

Although H-PGDS has been described as a monomeric protein (18,23), we recently demonstrated that H-PGDS is actually a homodimeric protein. Ultracentrifugation analysis revealed both rat and human H-PGDS's to be homodimers with a M_r of 45,000 to 49,000 in the presence or absence of Ca^{2+} or Mg^{2+} (**Table 2**).

Table 2. M_r value determined by ultracentrifugation analysis.

		Human H-PGDS	Rat H-PGDS
Theoretical Value		23343	23297
M_r, app	None	48013 ± 2147	44618 ± 3893
	5 mM $MgCl_2$	49026 ± 2174	45098 ± 5779
	1 mM $CaCl_2$	47996 ± 2792	48474 ± 6337

4) Inhibition of H-PGDS by HQL-79

We recently demonstrated that the orally active anti-allergic drug 4-benzhydryloxy-1-[3-(1*H*-tetrazol-5-yl)-propyl]-piperidine (HQL-79) is a specific inhibitor of human H-PGDS (27). Although HQL-79 was developed as an antagonist for histamine H1 receptors, a part of the anti-allergic and anti-asthmatic effects of HQL-79 was proposed to be mediated by the inhibition of PGD_2 production, because HQL-79 inhibited the conversion of PGH_2 to PGD_2 in crude extracts of mouse spleen (28). HQL-79 inhibited the activity of purified recombinant human H-PGDS with an IC_{50} of 6 μM, but had almost no effect on the activities of purified COX-1, COX-2, L-PGDS or microsomal

PGE synthase-1 (mPGES-1) when used up to 300 μM (**Fig. 4**). As described above, Mg^{2+} activates human H-PGDS about 2-fold and increases its affinity for GSH about 4-fold. In the absence of Mg^{2+}, the IC_{50} value of HQL-79 was increased about 3-fold, from 6 μM to 16 μM.

Kinetic analysis revealed that HQL-79 inhibited the H-PGDS activity in a competitive manner against PGH_2 (**Fig. 5A**), giving a *Ki* of 5 μM, and in a non-competitive one against GSH (**Fig. 5B**) with a *Ki* of 3 μM, in the presence of 1 mM $MgCl_2$. These results indicate that HQL-79 bound to the PGH_2-binding site but not to the GSH-binding site.

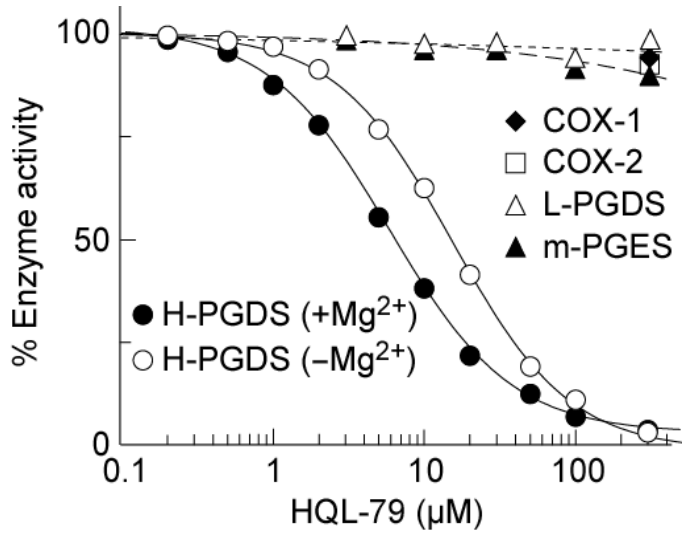

Figure 4. Selective inhibition of H-PGDS by HQL-79 (27).

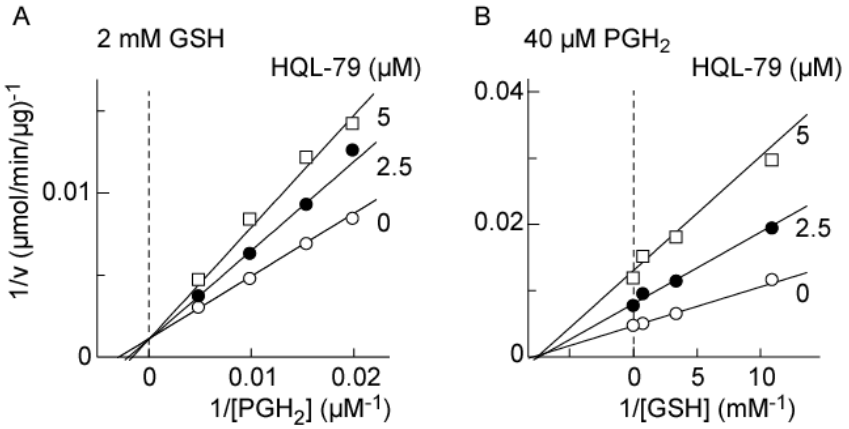

Figure 5. Kinetic analysis of inhibition of H-PGDS by HQL-79 (27).

5) Binding of HQL-79 to H-PGDS

Surface plasmon resonance (SPR) analysis showed that HQL-79 bound to H-PGDS in a concentration-dependent, saturable, and Mg^{2+}- and GSH-accelerated manner and dissociated from the enzyme-inhibitor complex immediately when washed (**Fig. 6A**). In the presence of 2 mM $MgCl_2$ and 2 mM

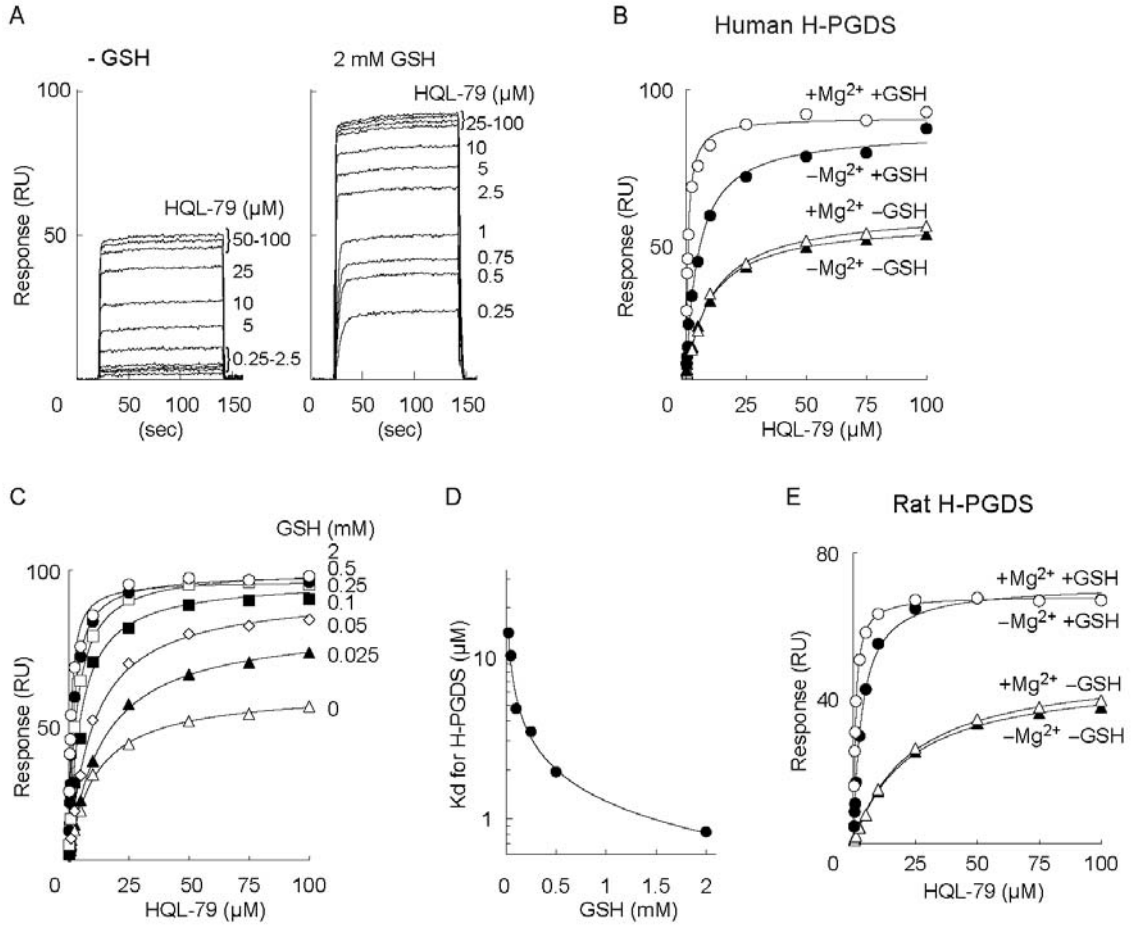

Figure 6. SPR analysis of binding of HQL-79 to H-PGDS (27).

GSH, HQL-79 bound to human H-PGDS in a concentration-dependent manner, with almost complete saturation up to 25 μM (**Fig. 6B**). From the association and dissociation curves, the K_d for HQL-79 was calculated to be 0.8 μM. In the absence of $MgCl_2$ and in the presence of 2 mM GSH, the HQL-79 binding to human H-PGDS significantly decreased, showing saturation at 50 μM and a K_d of 5 μM, indicating that the affinity of H-PGDS for HQL-79 decreased 6-fold in the absence of $MgCl_2$. In the absence of GSH, the HQL-79 binding decreased the total capacity to about 50% and increased the K_d to 11 μM in the presence of $MgCl_2$ and to 10 μM in its absence.

When we determined the GSH-dependency of the HQL-79-binding to human H-PGDS in the presence of $MgCl_2$, the binding affinity increased in a GSH concentration-dependent manner (**Fig. 6C**). The half-effective concentration of GSH for an increase in the affinity for HQL-79 and a decrease in the K_d was calculated to be 0.09 mM (**Fig. 6D**), which is similar to the K_m of the H-PGDS activity for GSH (0.14 mM), suggesting that GSH binding to the catalytic site of H-PGDS was involved in the increase in the binding affinity for HQL-79.

Rat H-PGDS showed an HQL-79-binding curve with a K_d of 0.7 μM. Similar to the human enzyme, in the absence of $MgCl_2$ the rat H-PGDS showed a 5-fold decrease in the binding affinity for HQL-79, giving the K_d value of 3.4 μM, without changing the maximum binding capacity. In the absence of GSH, the rat enzyme decreased the total binding capacity to about 50% and increased the K_d value to 22 μM in the presence of $MgCl_2$ and to 21 μM in its absence (**Fig. 6E**).

6) Functional coupling between H-PGDS and COX

HQL-79 inhibited either antigen- or Ca^{2+}-ionophore (A23187)-induced production of PGD_2 from [1-^{14}C] arachidonic acid in rat mastocytoma RBL-2H3 cells (**Fig. 7**) and human megakaryocytes in a concentration (3-300 μM)-dependent manner, both of which express predominantly H-PGDS. However, the production of other [^{14}C]-labeled metabolites was not inhibited by HQL-79 used up to 300 μM. This effect was quite different from that of indomethacin, which inhibited the production of all PGs. Moreover, HQL-79 had no effect on the production of PGD_2 by L-PGDS-over-expressing HEK-293 cells or human TE-671 cells (27), both of which predominantly express L-PGDS.

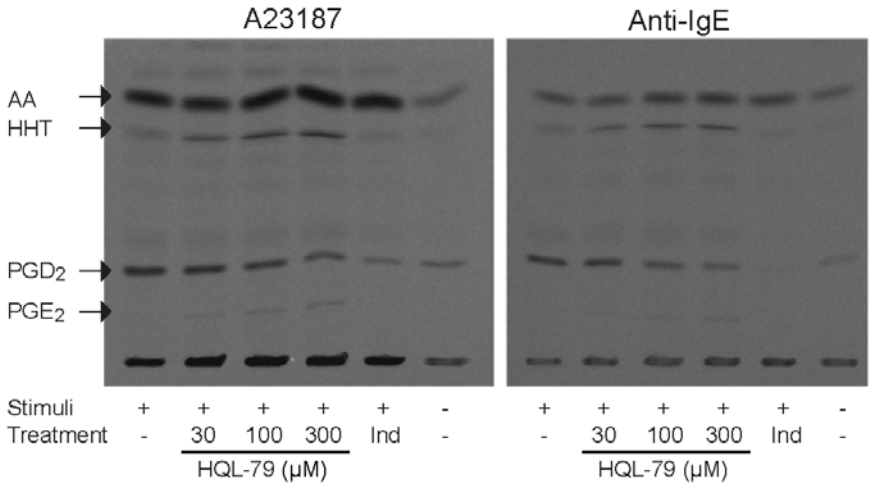

Figure 7. Selective inhibition of production of ^{14}C-PGD_2 in RBL cells by HQL-79 (27). AA, arachidonic acid; HHT, 12-hydroxyheptadecatrienoic acid; and Ind, indomethacin.

The IC_{50} value of HQL-79 for inhibition of PGD_2 production in megakaryocytes was calculated by EIA to be 102 μM (**Fig. 8**). HQL-79 at a concentration of 300 μM decreased PGD_2 production to 3.1 ng/10^6 cells from 10.1 ng/10^6 vehicle-treated cells; whereas it increased PGE_2 production to 0.32 ng/10^6 cells from 0.17 ng/10^6 vehicle-treated cells and decreased $PGF_{2\alpha}$ production to 0.23 ng/10^6 cells from 0.34 ng/10^6 vehicle-treated cells. HQL-79 tested up to 300 μM did not affect at all the production of PGD_2, PGE_2 or $PGF_{2\alpha}$ in the L-PGDS-over-expressing HEK-293 cells.

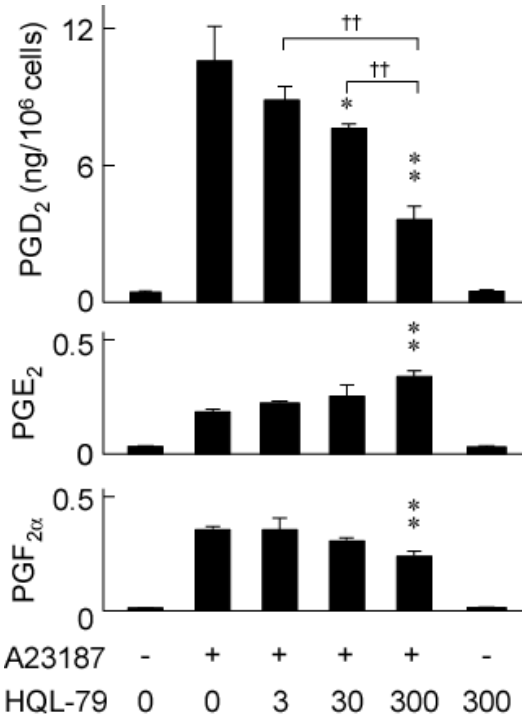

Figure 8. Selective inhibition of production of PGD_2 in megakaryocytes by HQL-79 (27). Selective inhibition by HQL-79 of PGD_2 accumulated in the culture medium of MEG-01S cells. The amounts of PGD_2, PGE_2, and $PGF_{2\alpha}$ were measured by EIA. Data represent the mean ± SEM (n=4). *p<0.05, **p<0.01 as compared with the value in the absence of HQL-79. ††p<0.01 as compared with the value in the presence of 300 μM HQL-79 (Dunnett's test).

These results indicate that the inhibition of H-PGDS decreased PGD_2 production selectively without significantly affecting the biosynthesis of other PGs. Once the downstream H-PGDS was inhibited, the upstream COX was also inhibited, suggesting that H-PGDS and COX were functionally tightly engaged with each other (**Fig. 9**). In this sense, HQL-79 is an even better PG-blocking compound than those available today (29). Non-steroidal anti-inflammatory drugs (NSAIDs) are the most widely used as anti-inflammatory drugs that ameliorate pain, fever, and inflammation by blocking PG production. However, NSAIDs inhibit the production of all prostanoids, including the cytoprotective and anti-inflammatory PGs (**Fig. 9**). For example, aspirin and indomethacin induce gastrointestinal toxicity by blocking PGE_2 production. The anti-inflammatory action of PGE_2 mediated by EP3 receptors was also very recently reported (30). We previously demonstrated that PGD_2 produced by L-PGDS prevents neuronal and oligodendroglial apoptosis during neuroinflammation in a genetic demyelination mouse model, i.e., twitcher (31). Thus, HQL-79 may be predicted to selectively suppress the inflammatory reaction mediated by H-PGDS-catalyzed PGD_2 without various side effects caused by the suppression of cytoprotective and anti-inflammatory PGs.

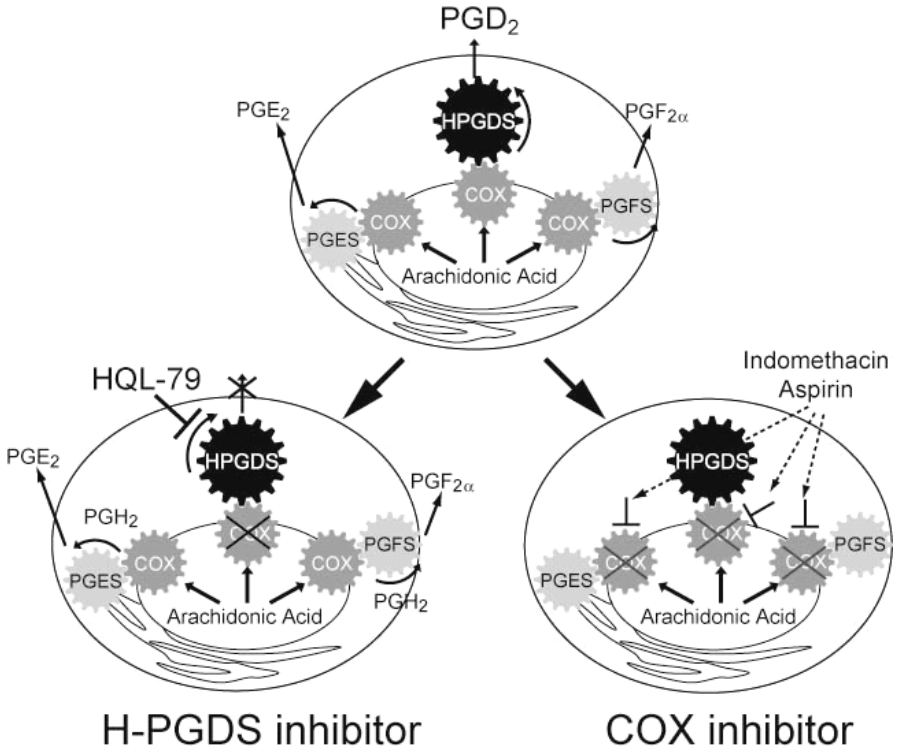

Figure 9. Comparison of selective inhibition of PGD_2 production by HQL-79 with total inhibition of PG production by Ind. indomethacin.

7) Tissue and cellular distribution of H-PGDS

Immunoabsorption analysis of the PGDS activity in various rat tissues with anti-H-PGDS antibodies revealed that H-PGDS contributes to the production of PGD_2 in the spleen, thymus, intestine, and various peripheral tissues of rats (32). Northern blot analysis showed that the tissue distribution profile of the mRNA for H-PGDS highly deviated among various species including rats (33), humans, mice (34), and chickens (35). However, H-PGDS was highly expressed in the oviduct of all 3 mammalian species, indicating that H-PGDS plays an important role in the female genital organ.

H-PGDS is immunohistochemically or immunocytochemically localized in Langerhans cells in the skin (36), Kupffer cells in the liver, dendritic cells in the thymus and intestine (37), mast cells (1) of variety of rat and human tissues; human megakaryocytes (38), activated Th2 cells (2), and eosinophils (39); microglia of the mouse brain (4,41); and necrotic muscle of *mdx* mice (I.M., Y.U.; unpublished results) or patients with Duchenne's muscular dystrophy or polymyositis (41).

Evolutional properties of H-PGDS

We have already obtained the full-length cDNA for rat H-PGDS (33) followed by that for the human and mouse enzymes (34). The cDNA encodes a

protein composed of 199 amino acid residues with a calculated M_r of 23,297, 23,343, and 23,226 for the rat, human, and mouse enzymes, respectively. The first N-terminal methionine is cleaved from the mature enzyme. The cDNA for the chick homolog was isolated by Thompson et al. (35).

A database search of the protein primary structure revealed H-PGDS to be a member of the GST family, as predicted by the results obtained by partial amino acid sequence analysis. The amino acid sequence of H-PGDS was similar to those of all GST isozymes from the previously known 5 classes: alpha, mu, pi, sigma, and theta (**Fig. 10**), showing weak similarity (<30% identity) to mammalian GST isozymes, yet moderate similarity (32% to 40% identity) to the insect and fluke GST, and the highest identity to GSTs of the house fly (*Musca domestica*, 40% identity) and pig roundworm (*Ascaris suum*, 39% identity) in the multiple sequence alignment.

In a phylogenetic tree, H-PGDS formed a subcluster with members of the sigma class GST including S-crystallins from cephalopods (**Fig. 11**). The sigma class GSTs were previously reported to be present in invertebrates such as insects, cephalopods, flukes, and nematodes. Thus, H-PGDS is a novel vertebrate homolog of the sigma class of the GST family. Among members of the sigma-class GST family, H-PGDS is the most related to *C. elegans* GST (σ).

Members of the alpha, mu, and pi-class GSTs and squid GST (σ) of the sigma-class GST have the ability to convert PGH_2 to a mixture of PGD_2, PGE_2, and $PGF_{2\alpha}$ in the presence of GSH (42,43). However, their PGD synthase activity was lower than their PGE synthase and PGF synthase activities. Therefore, we propose that the H-PGDS gene evolved from a common ancestor of the

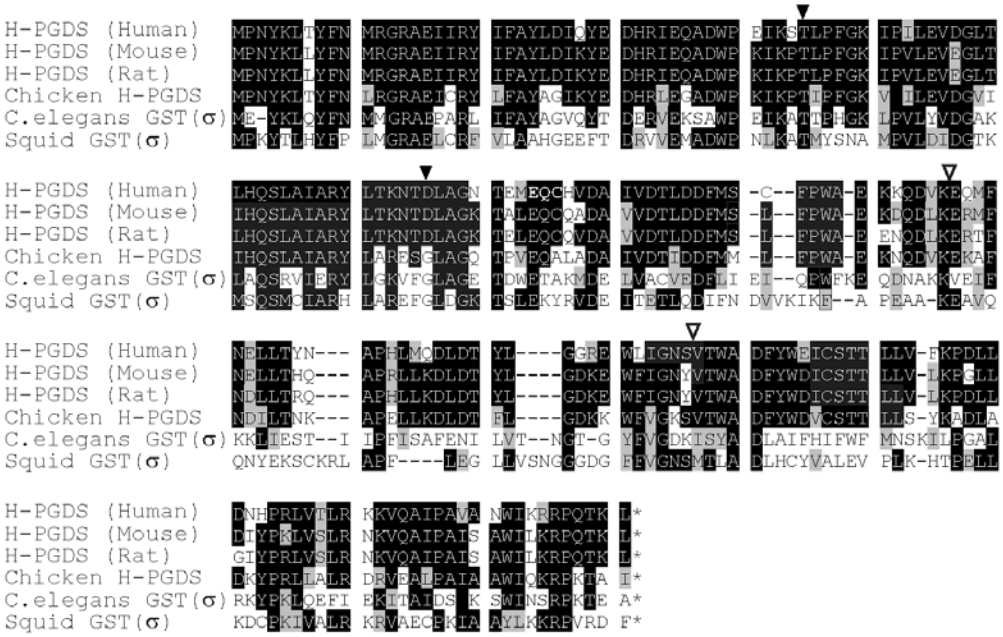

Figure 10. Homology of H-PGDS with members of GST family (34).

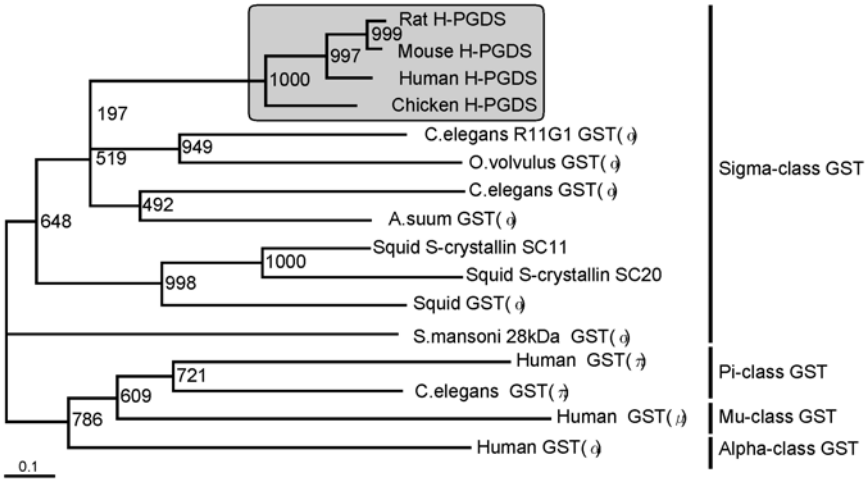

Figure 11. Phylogenetic tree of H-PGDS and GSTs (34).

invertebrate sigma-class GSTs, and acquired specifically PGD synthase activity during its evolution. Metal activation of the enzyme activity was not observed in any other GST isozymes in the alpha, mu, pi, and sigma classes or in the sigma class GST from *Schistosoma mansoni*, thus indicating that the metal activation is specific to H-PGDS among the GST family. H-PGDS is a unique Mg^{2+}-containing GST.

Crystallographic structure of H-PGDS

We have determined the X-ray crystallographic structures of H-PGDS of 4 distinct complexes, as summarized in **Table 3** (26, 27, 34).

Table 3. Summary of crystallographic structures of 4 distinct complexes of H-PGDS.

Species	Rat	Human	Human	Human
Ligand	GSH	Ca^{2+}, GSH	Mg^{2+}, GSH	HQL-79, Mg^{2+}, GSH
Space group	$P3_121$	$P2_1$	$P2_1$	$P1$
Cell dimensions (Å)	a =56.5,	a = 48.8,	a = 48.8,	a = 46.9,
	b = 56.5,	b = 47.3,	b = 47.3,	b = 49.1,
	c = 233.4,	c = 183.8	c = 183.8	c = 93.4
(deg.)	α = 90.0,	α = 90.0,	α = 90.0,	α = 85.8,
	β = 90.0,	β = 97.8,	β = 97.8,	β =88.7,
	γ = 120.0	γ = 90.0	γ = 90.0	γ = 90.0
Resolution (Å)	6.0 – 2.3	37.3 – 1.8	30.9 – 1.7	35.0 – 1.45
No. of reflections used	17,811	65,599	72,114	121,073
No. of water molecules	99	1,089	983	1,398
R_{cryst} (%)	20.4	19.3	21.0	19.2
R_{free} (%)	28.9	22.6	24.1	20.7
R.m.s. deviation of				
bond lengths (Å)	0.01	0.005	0.006	0.012
bond angles (deg.)	1.613	1.1	1.0	1.3
Reference	*(33)*	*(26)*	*(26)*	*(27)*

1) Rat enzyme as a binary complex with GSH

We first determined the crystal structure of the rat H-PGDS.GSH complex at 2.3 Å resolution by the multiple isomorphous replacement method (33). The recombinant rat H-PGDS was crystallized in a trigonal $P3_122$ form. The crystal was obtained as a homodimer in an asymmetric unit, and each monomer was complexed with 1 GSH molecule (**Fig. 12**). The monomers were related by a non-crystallographic 2-fold axis. The dimer interaction showed the "lock-and-key" complimentarity feature of a hydrophobic surface of Phe48 with a limited number of the electrostatic interactions (**Fig. 12**), which is commonly observed in various GSTs.

The dimensions of the H-PGDS monomer are about 50 x 50 x 30 Å, and the overall folding motif is the same as those of GSTs. The monomer is constructed from 2 domains with a prominent interdomain cleft (**Fig. 12**); the N-terminal domain (amino acid residues 1–71) and the C-terminal domain (82–199) are connected by the residues 72–81 including 2 turn structures (72–75 and 76–79). The N-terminal domain contains a 4-stranded β sheet and 3 α helices, arranged in a βαβαββα motif, in which the β1 and β2 are parallel and the β1 and β3, and the β3 and β4, are antiparallel. The α1 and α3 helices make the dimer interface with the α4, α6, and α8 of the counterpart in the dimer. The loop structure (46–52) bends at the position of Pro52 to the outside of the enzyme, which is the GSH binding site. The angle between the directions of the loop and the β3 backbone is approximately 90°, so that the side chains of the loop residues are exposed to the solvent with the Ile51 residue in *cis*-conformation, resulting in the formation of a GSH-binding dimple. The C-terminal domain is composed of 5 α helices, in which the α4, α5, and α6 make an α-helix bundle. The long α5 bends at the position of Gln123. In the connecting loop of the α4 and α5 helices, the backbone between Ser100 and Trp104 is kinked to compensate for the α4, which is shorter than those of other GSTs in the amino acid alignment.

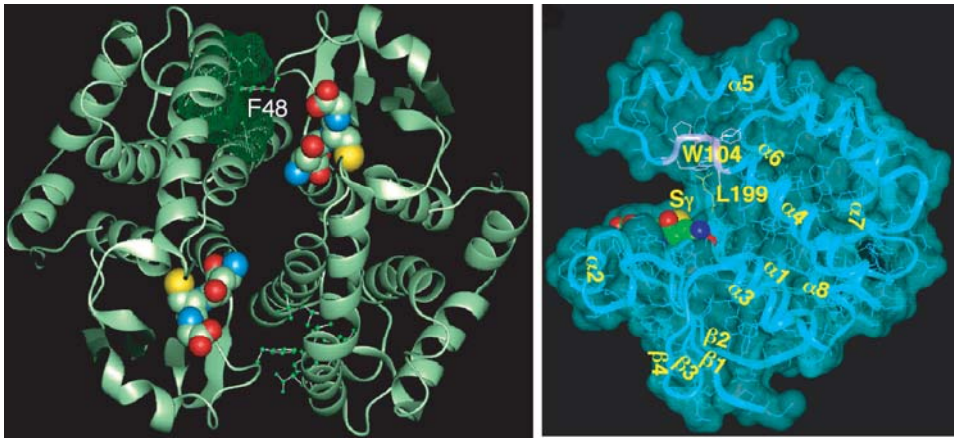

Figure 12. Crystallographic structure of rat H-PGDS as a binary complex with GSH (33).

GSH is bound to the side of the N-terminal domain (**Fig. 13**) by forming 2 and 8 hydrogen bonds to the atoms of the protein backbone and side chain, respectively, similar to other GSTs. The cysteinyl backbone of GSH interacts with that of *cis*-Ile51 of the N-terminal domain via hydrogen bonds in an antiparallel β-sheet manner. The amino nitrogen of the γ-glutamate residue of GSH forms hydrogen bonds with both of the carboxyl oxygens of the Asp97 side chain of the other H-PGDS molecule in the dimer. The Sγ atom of GSH and the Oη of Tyr8 show a hydrogen bonding distance of 3.1 Å. All these residues are highly conserved among the members of the GST family.

The prominent cleft including the GSH binding site between the 2 domains is the catalytic pocket. The interdomain cleft expands to a wide and deep pocket (pocket 1) behind the GSH binding site with the longest loop eaves of the α4 and α5 helices. At the entrance of pocket 1, the indole ring of Trp104 forms a ceiling on the C-terminal domain, since the indole ring is directed parallel to the α4 helix extended by the kinked backbone including Trp104. Pocket 1 has a path to a branched cavity consisting of another pocket (pocket 2) and a narrow tunnel. Pocket 1 also opens to a third pocket (pocket 3) on the outer surface due to the short C-terminal end of H-PGDS. There is a straight path from the outside of the protein to pocket 2 via pockets 3 and 1.

As for the dimensions of the cavities, pocket 1 is 5 Å in depth by 6 Å in width and opens to the GSH binding site. Pocket 2 is 4 Å in depth and 6 Å in width and is lined with hydrophilic residues in contrast to pockets 1 and 3, whose surfaces are hydrophobic with many aromatic side chains. In the bottom of pocket 2, there are 2 bound water molecules that are 2.9 Å apart; and they form hydrogen bonds with the 0η of Tyr152 and the Nζ of Arg14, which are at the distances of 8.7 Å and 8.1 Å, respectively, from the Sγ atom of GSH. The electrostatic potential on the surface within the cleft including GSH is positive around the guanidino group of Arg14, negative along GSH, and neutral in the other part.

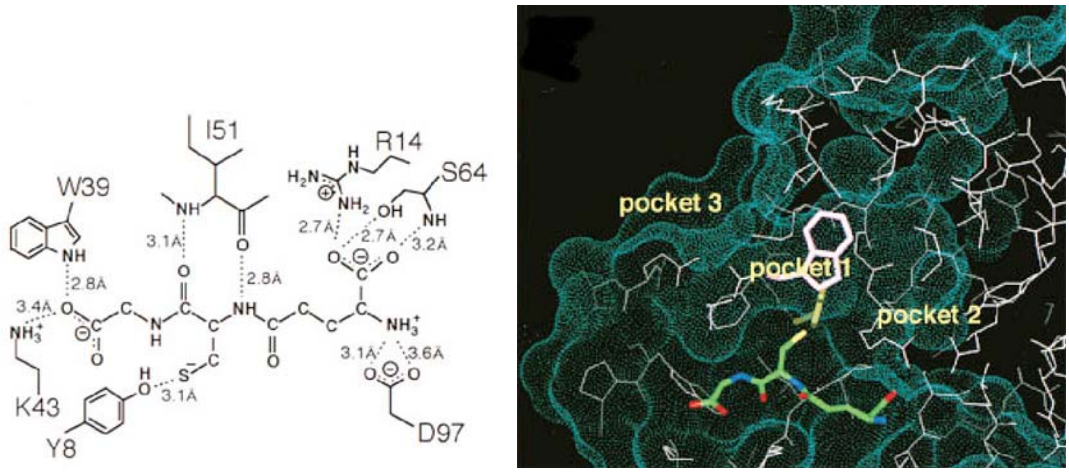

Figure 13. GSH-binding to the catalytic cleft of rat H-PGDS (33).

2) Human H-PGDS as the ternary complex with GSH and Ca^{2+} or Mg^{2+}

We then obtained monoclinic $P2_1$ crystals of human H-PGDS in the presence of Ca^{2+} and GSH, and determined the structure at 1.8 Å resolution (26). The asymmetric unit of the crystal lattice contained 2 enzyme-dimers, designated Mol-A/Mol-D and Mol-C/Mol-B (**Fig. 14A**). The human H-PGDS dimer structure (**Fig. 14B**) was identical to that in the trigonal crystal of rat H-PGDS (**Fig. 12**), and the overall fold of each H-PGDS subunit was essentially the same as that of other GSTs and rat H-PGDS.

The subunits in the dimers had similar overall folds: the r.m.s. deviations were 0.23 Å for Mol-A/Mol-B, 0.42 Å for Mol-A/ Mol-C, 0.29 Å for Mol-A/Mol-D, 0.43 Å for Mol-B/Mol-C, 0.30 Å for Mol-B/Mol-D, and 0.35 Å for Mol-C/Mol-D for all Cα atoms except for the region of helix α5. Specifically, Tyr122 in helix α5 of Mol-A and Mol-B was clearly distinct from that of Mol-C and Mol-D; Tyr122 of Mol-A and Mol-B but not that of Mol-C and Mol-D could make a hydrogen bond with His87 in the neighboring dimers in the crystal. Moreover, the structure of the glycine residue of the bound GSH in Mol-B was clearly different from that of Mol-A, Mol-C, and Mol-D.

The high-resolution structure revealed Ca^{2+} to be at the center of the dimer interface (**Fig. 14B**). The Ca^{2+}-binding site consisted of pairs of Asp93, Asp96, and Asp97 from each monomer. These 6 aspartates formed an acidic cluster at the dimer interface, and the residues from each pair were related *via* a non-crystallographic two-fold symmetry axis at the center of the dimer. The Ca^{2+}-binding site was at a hinge portion between the N- and C-terminal domains of the subunit (**Fig. 14C**). The Ca^{2+} ion was directly coordinated by 5 water molecules (W1–W3, W5, and W6) and Asp96 in Mol-C or Mol-D (**Fig. 15**). Asp96 from Mol-A or Mol-B interacted with the coordinated water molecule W6; and Asp93 and Asp97, with the Ca^{2+} ion through water molecules (W5 and W1 and W2, respectively). The distance between O1(Asp96) of Mol-C or Mol-D and Ca^{2+} was 2.8 Å; whereas that between Ca^{2+} and W6 was 2.0 Å, and that between W6 and O1(Asp96) of Mol-A (or Mol-B) was 2.5 Å. In the dimer, each of the O2 (Asp96) atoms made 2 hydrogen bonds with the guanidium nitrogen atoms of Arg14 in the same subunit. In turn, each of the N2 (Arg14) atoms formed a hydrogen bond with an Oγ(Ser100) in the same subunit, but the observed distances were different: 3.0 Å for Mol-A or Mol-B and 2.6 Å for Mol-C or Mol-D. The Arg14 residue was involved in the activation of the thiol of GSH and in recognition of the ω-chain of the substrate PGH_2. Thus, Ca^{2+}, Asp96, Arg14, and Ser100 formed a hydrogen-bonding network at the active site of human H-PGDS.

The structure of human H-PGDS in the presence of Mg^{2+} was also determined, at 1.7 Å resolution (26). The space group of the crystal and the

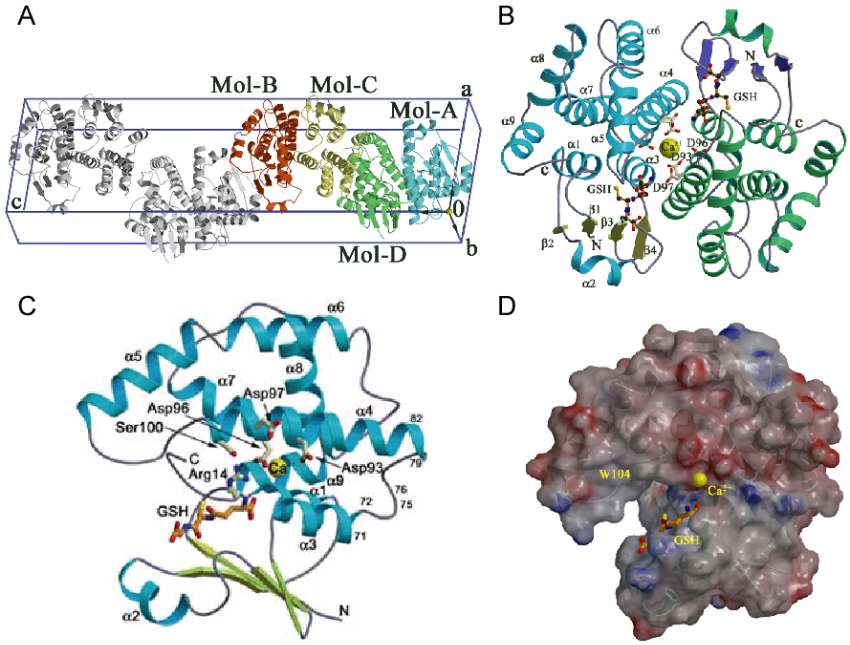

Figure 14. Crystallographic structure of human H-PGDS as ternary complexes with GSH and Ca^{2+} (26).

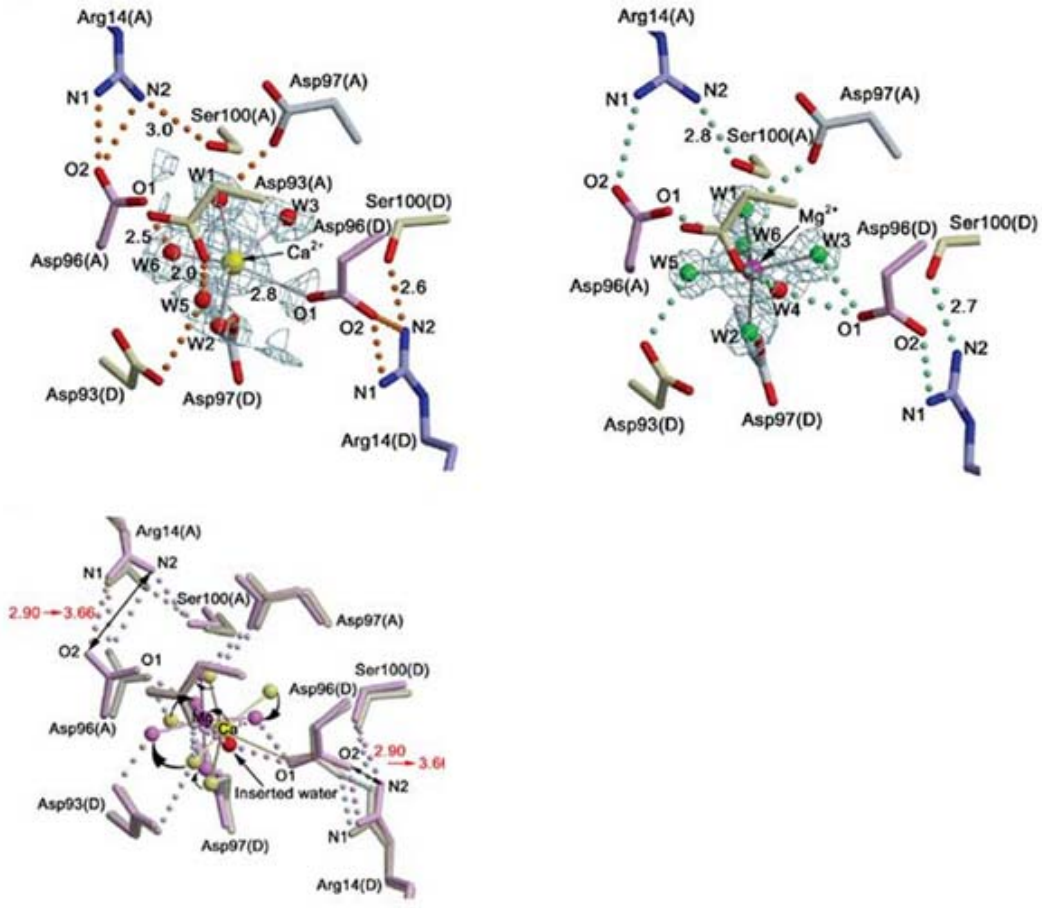

Figure 15. The metal coordination structures of human H-PGDS (A), Mol-A; (D), Mol-D.

overall structure were the same as those of the Ca^{2+}- bound enzyme. Mg^{2+} occupied virtually the same metal-binding site at the dimer interface as observed in the Ca^{2+}-bound form. However, Mg^{2+} was octahedrally coordinated by 6 water molecules (W1–W6) at the dimer interface (**Fig. 15**). Because the ionic radius of Mg^{2+} (0.65 Å) is shorter than that of Ca^{2+} (0.99 Å), one more water molecule (W4) was inserted into the Mg^{2+} coordination structure. The Asp96 from Mol-C or Mol-D interacts with 2 coordinated water molecules (W3 and W4), whereas the Asp96 from Mol-A or Mol-B interacted with 1 water molecule (W6). In contrast to the Ca^{2+}-bound structure, the organization of water molecules around Mg^{2+} was symmetric. The hydrogen-bonding networks around the metal ion observed in the Ca^{2+}-bound structure were perturbed upon Mg^{2+} binding. As a consequence of the binding, the position of Mg^{2+} was shifted by 0.68 Å from that of Ca^{2+} toward the center of the dimer, and W4 was inserted in the Mg^{2+} coordination structure. These two structural alterations increased the distance between the 2 O1(Asp96) atoms from 6.8 Å to 7.6 Å. In addition to the rearrangement of the water structure surrounding the metal ion, the hydrogen-bonding network between Arg14 and Asp96 was also markedly changed. In the Ca^{2+}-bound form, both O2(Asp96) atoms formed hydrogen bonds with the guanidium nitrogen atoms of Arg14 (N1 and N2); whereas in the Mg^{2+}-bound form, only 1 hydrogen bonded to the N1 of Arg 14 was observed. The average distance of N2(Arg14)-O2(Asp96) increased from 2.90 Å (2.69–3.05Å) in the Ca^{2+}-bound form to 3.66 Å (3.49–3.91 Å) in the Mg^{2+}- bound form because of the loss of this hydrogen bond. Moreover, the average distance between Ser100 and Arg14 in Mol-A or Mol-B changed from 3.01 to 2.82 Å. Although the conformations of GSH, Ser100, and Trp104 were identical in both metal-bound forms, the guanidium plane of Arg14 and the carboxyl plane of Asp96 changed by 11.1° and 11.9°, respectively (**Fig. 15**). The side chain of Arg14 rotated upon Mg^{2+} binding, producing the metal ion effect on the reactivity as described below.

3) Human H-PGDS as the quaternary complex with GSH, Mg^{2+}, and HQL-79

We recently determined the crystal structure of human H-PGDS as a quaternary complex with Mg^{2+}, GSH, and HQL-79 (27). The crystal of the complex was obtained in a space group of *P*1, in which 2 dimer molecules of H-PGDS (Mol-A and D, Mol-B and C) were located in an asymmetric unit (**Fig. 16A**). The 2-dimer packing in the HQL-79 complex of human H-PGDS was essentially the same as that of the Ca^{2+}- or Mg^{2+}-bound native form without inhibitors.

The high-resolution structure gave a clear electron-density map for the HQL-79 molecule at a resolution of 1.45 Å (**Fig. 16B**). Four independent

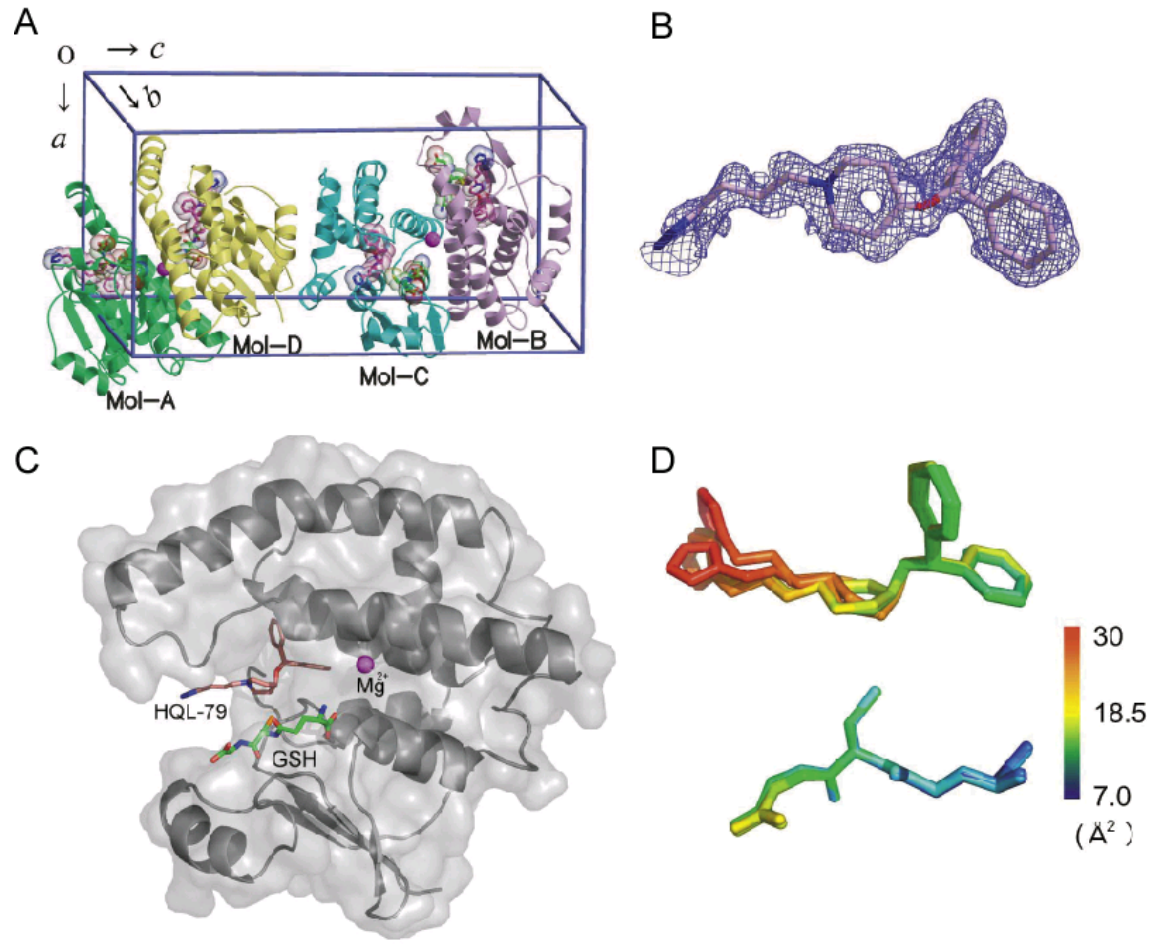

Figure 16. Crystallographic structure of human H-PGDS as a quaternary complex with GSH, Mg^{2+}, and HQL-79 (27).

molecules of HQL-79 and 4 of GSH were well superimposed within Mol-A to -D of human H-PGDS, in which the tetrazole tail of HQL-79 showed slightly different conformations among the 4 molecules. Among the 4 molecules, the tetrazole tail of Mol-A and -B on the out side in the packing unit (**Fig. 16A and D**) was more deviated than that of Mol-C and -D on the inside, probably due to the interaction with molecules in the neighboring packing units.

The HQL-79 molecule was inserted in the catalytic cleft between Trp104 and GSH (**Fig. 16C**). No steric hindrance was detected between HQL-79 and the GSH molecule, being completely consistent with the kinetic analyses showing that HQL-79 was a competitive inhibitor against the substrate, PGH_2, and a non-competitive inhibitor of GSH (**Fig. 5**).

Among the 3 pockets (pockets 1, 2, and 3; **Fig. 13**) in the catalytic cleft of H-PGDS, phenyl-1 and phenyl-2 of the diphenyl of HQL-79 penetrated into pocket 1 and pocket 2, respectively (**Fig. 17**). The HQL-79 molecule was stabilized by weak hydrogen bonding with Met99, Phe102, Trp104, and Tyr152 located within a distance of 3.5 Å. and by Arg14, Thr159, and

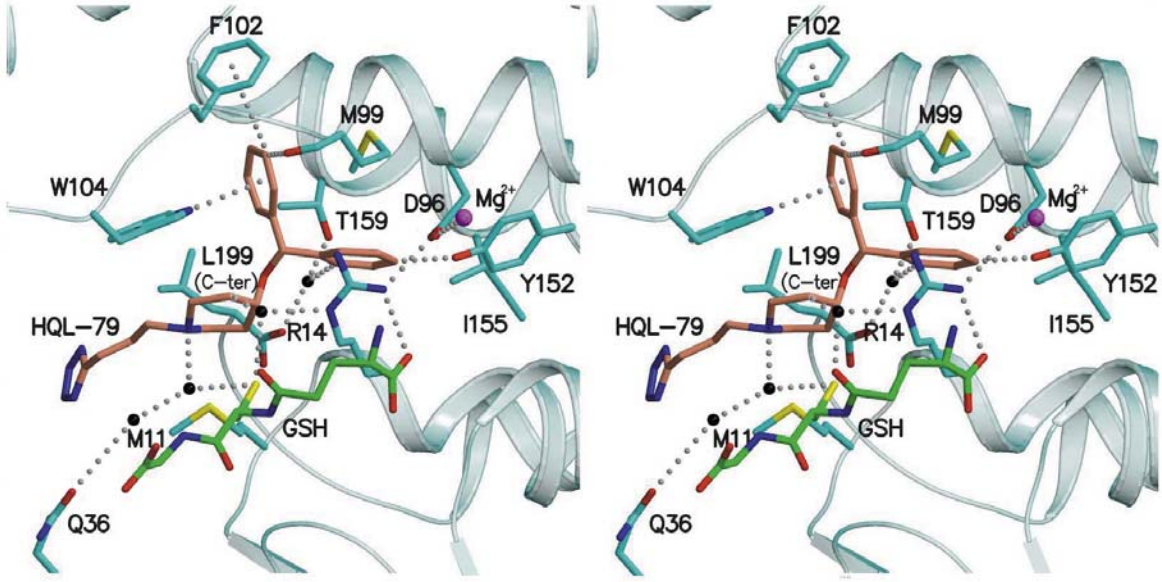

Figure 17. HQL-79 having penetrated into pocket 1 and pocket 2 of the catalytic cleft of human H-PGDS (27).

Leu199, including GSH (by non-bonding interactions including salt bridges and hydrogen bonding) through water molecules (colored black in **Fig. 7**). The tetrazole ring of HQL-79 was located at the entrance of pocket-3 and did not directly interact with the positively charged amino acid cluster of Lys112 and Lys198 in this pocket. No direct interaction was detected around the tetrazole ring, suggesting that the tetrazole group of HQL-79 interacted with Lys112 and Lys198 via diffusible water molecules in pocket-3.

In the catalytic cleft, a phenyl ring of the diphenyl of HQL-79 exhibited van der Waals interaction with the indole ring of Trp104, including weak hydrogen bonding with the ring nitrogen. In comparison with the native structure of the enzyme, the HQL-79 molecule penetrated into the ceiling of the catalytic cleft and pushed out the indole ring of Trp104, resulting in the rotation of the indole ring by 48 degrees with a 4.3 Å shift. The movement of Trp104 induced twisting of loop7, which was linked to the long kinked α5-helix. The C_α carbon of Lys107 located at the top of the α5-helix moved 4.4 Å, the number of which was extremely larger than the r.m.s. deviation of 0.42 Å for the C_α atoms between the complex and the native form.

Analyses by site-directed mutagenesis

1) H-PGDS and GST activities in mutants

Based on the crystal structure of rat H-PGDS, we prepared 10 mutants for the amino acid residues facing the catalytic cleft (**Fig. 18A**), i.e., the $Tyr^{8}Phe$, $Arg^{14}Lys/Glu$, $Trp^{104}Ile$, $Lys^{112}Glu$, $Tyr^{152}Phe$, $Cys^{156}Leu/Tyr$, $Lys^{198}Glu$, and

Leu[199]Phe mutants, and determined the H-PGDS and GST activities (44). The crystallographic topology of those amino acid residues within the catalytic cleft is well conserved between rat H-PGDS and human H-PGDS.

There were 3 types of effects on the PGDS and GST activities (**Fig. 18B**). Both activities were retained in Lys[112]Glu, Tyr[152]Phe, Lys[198]Glu, and Leu[199]Phe mutants, indicating that Lys112, Tyr152, Lys198, and Leu199 residues were not essential for either activity of H-PGDS. Complete loss of only the PGDS activity was found in Cys[156]Leu/Tyr mutants, thus indicating that Cys156 involvement in construction of the PGH_2-binding pocket. Tyr[8]Phe, Arg[14]Lys/Glu, and Trp[104]Ile mutants completely lost both activities, suggesting that the Tyr8, Arg14, and Trp104 residues were important for the catalytic activity of H-PGDS.

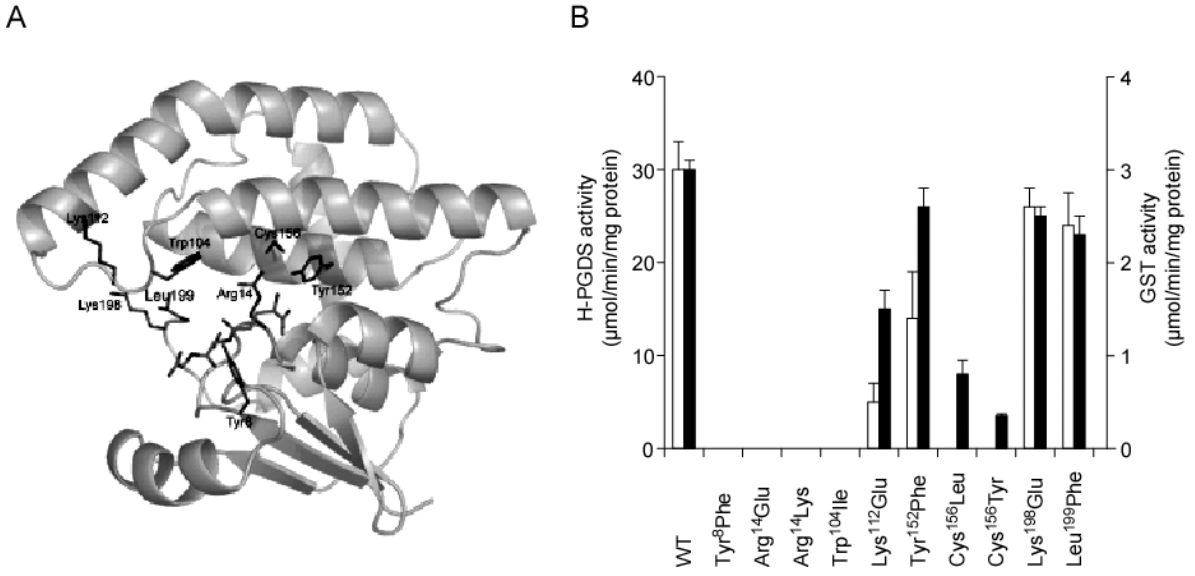

Figure 18. H-PGDS and GST activities of 10 mutants of rat H-PGDS. A. Positions of 10 amino acid residues facing the catalytic cleft. The side chains of amino acids that were mutated in this study are shown by gray sticks. **B.** Summary of the H-PGDS and GST activities of the 10 mutants (44).

2) Effects of mutation on GSH activation

The loss of PGDS and GST activities in some mutants was not attributable to the loss of GSH binding, because all of those mutant enzymes bound to GSH-Sepharose. Therefore, we examined the reactivity of the thiol group of GSH bound to the mutants with a thiol-modifying agent, 5,5'-dithiobis(2-nitrobenzoic acid), DTNB (**Fig. 19)**.

When wild-type rat H-PGDS was incubated with DTNB in the absence of GSH, no reaction was observed at pH 5.0, indicating that the 2 free cysteine residues in the wild-type protein were not titrated with DTNB. In solution with 0.5 mM GSH, DTNB was converted to 5-thio-2-benzoic acid at an initial rate

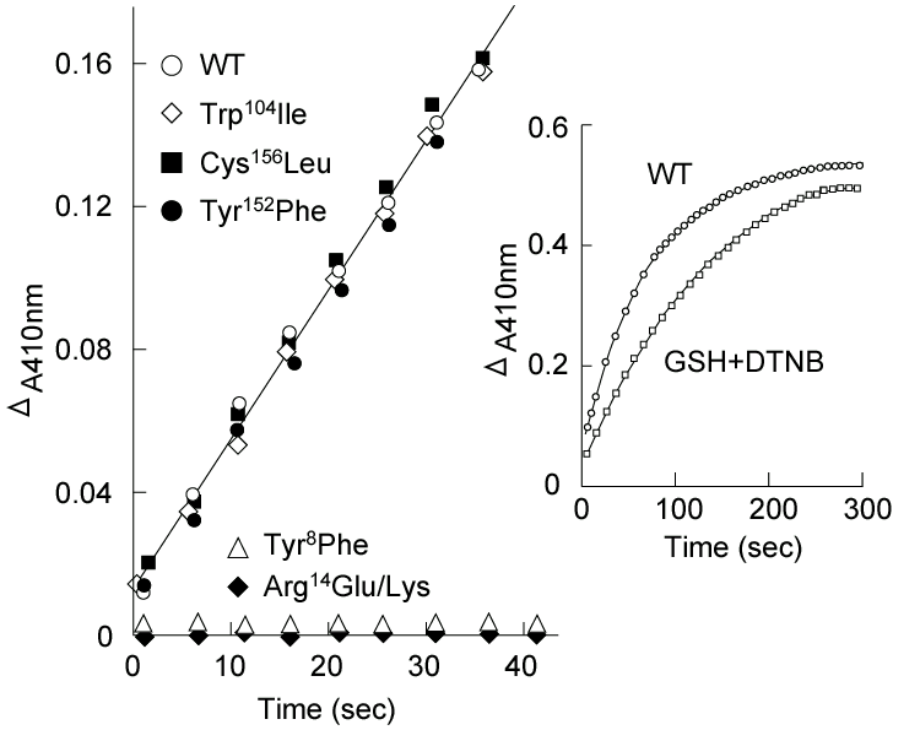

Figure 19. Effects of the mutations on GSH activation (44). The excess SH-selective reaction of the mutants W104I, C156L, Y152F, R14E/K, and Y8F including the wild-type enzyme with DTNB is shown after subtraction of the control reaction with no enzyme. The reaction rates for the K112E, C156Y, K198E, and L199F mutants with DTNB were identical to the rate of the wild-type enzyme. The R14K/E and Y8F mutants showed no excess reactivity with DTNB. The inset represents the raw reaction curves during 5 min of reaction of the wild-type enzyme (WT) and 1 mM GSH + 0.05 mM DTNB as the control reaction (open square). The concentrations used were as follows: enzymes, 0.1 mM; GSH, 0.5 mM; and DTNB, 0.05 mM.

of 15 mM/min (**Fig. 19** inset). The addition of the wild-type enzyme or the $Trp^{104}Ile$, $Lys^{112}Glu$, $Tyr^{152}Phe$, $Cys^{156}Leu/Tyr$, $Lys^{198}Glu$ or $Leu^{199}Phe$ mutant increased the reaction rate exactly 2-fold, indicating that GSH had been activated (44). The reaction rates for the K112E, C156Y, K198E, and L199F mutants with DTNB were identical to the rate of the wild-type enzyme. The $Trp^{104}Ile$ mutant without either H-PGDS or GST activity bound GSH and activated it to the thiolate anion. However, no enhancement of thiol activity was observed with $Tyr^{8}Phe$ and $Arg^{14}Lys/Glu$ mutants, suggesting that Tyr8 and Arg14 residues are essential for activation of GSH to form the thiolate anion within the catalytic cleft of H-PGDS.

3) Effects of mutation on metal activation

We generated the $Asp^{93}Asn$, $Asp^{96}Asn$, and $Asp^{97}Asn$ mutants to clarify the contribution of Asp93, Asp96, and Asp97 residues in the metal-binding site to the activation of H-PGDS by the Mg^{2+} ion. As expected from our structures,

none of the mutants was activated by Mg^{2+} ion (**Fig. 20**). Neither the $Asp^{93}Asn$ nor the $Asp^{97}Asn$ mutant showed increased affinity for GSH in the presence of Mg^{2+}. The affinity of the $Asp^{96}Asn$ mutant for GSH was already increased irrespective of Mg^{2+}, differing from the wild-type enzyme and the 2 other mutants. The $Asp^{97}Asn$ mutation decreased the activity to about 1% of that of the wild-type enzyme when the transformant *E. coli* were cultured at 37°C (26). However, when the trasformants were cultured at 16°C, the purified enzyme showed almost the same activity as the wild-type enzyme, indicating that Asp97 residue was important for the stabilization of the enzyme in *E. coli*.

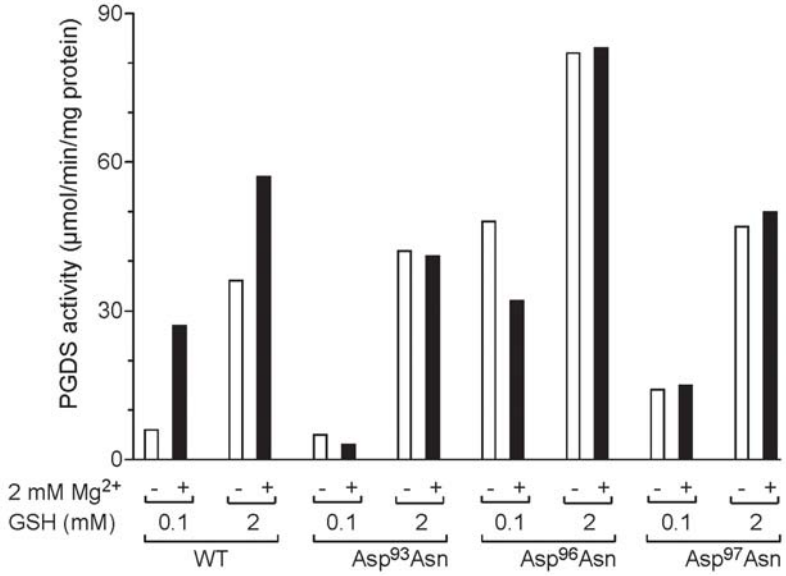

Figure 20. Effects of the mutations on the activation of H-PGDS by Mg^{2+} (26).

4) Catalytic mechanism of H-PGDS

Our mutational study revealed that Arg14 was involved in the stabilization of the thiolate anion of GSH bound to H-PGDS. The activated thiolate probably attacks the O11 of the endoperoxide group of the substrate PGH_2, and a hydrogen bond between the amide nitrogen of glycine from GSH and O9 of the endoperoxide group of PGH_2 may stabilize the bound PGH_2 molecule (**Fig. 21**, 46). The crystallographic structures revealed that the binding of Mg^{2+} led to the loss of 1 hydrogen bond between Asp96 and Arg14, as compared with the Ca^{2+}-binding enzyme (**Fig. 15**). This loss would be expected to increase the mobility of Arg14. Upon Mg^{2+} binding, Arg14 would become available to form a salt bridge or a hydrogen bonding network with the thiolate group of GSH to stabilize the negative charge, which might then accelerate the nucleophilic attack on the endoperoxide group of PGH_2. The mobility of Arg14 residue may also be improved in the $Asp^{96}Asn$ mutant, resulting in the higher activity of it than that of the wild-type enzyme in the absence of Mg^{2+}.

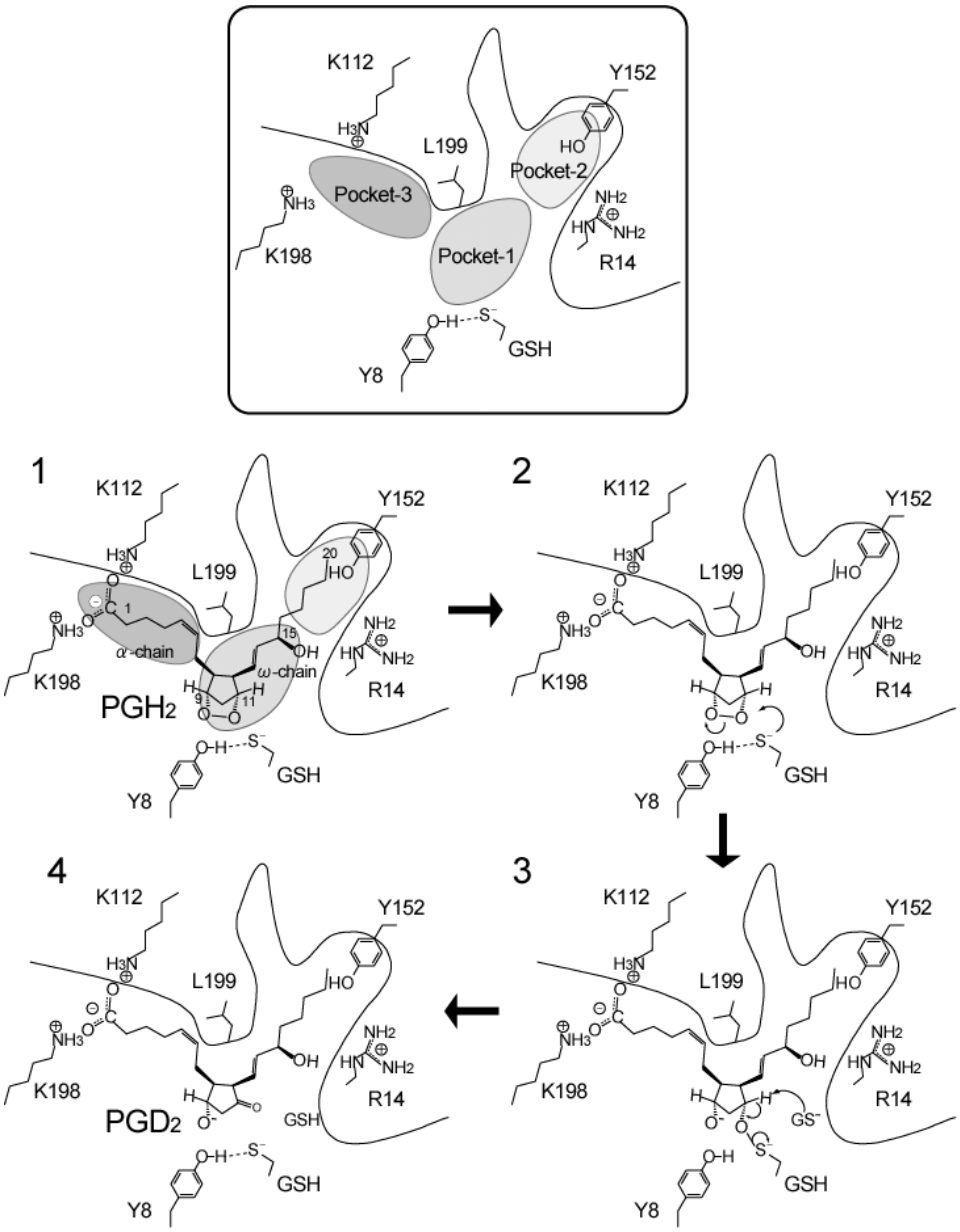

Figure 21. Catalytic mechanism of H-PGDS (46). A schematic drawing of the catalytic pocket of H-PGDS with PGH_2. Pockets 1, 2, and 3 are shaded. The thiolate anion of bound GSH attacks the oxygen at C11 of PGH_2 (panel 2). The putative reaction intermediate of PGH_2 with GSH is attacked by a certain base-like bulk GSH in solvent (panel 3) to produce PGD_2 in a sterically restricted manner (panel 4).

5) Effects of mutation on the HQL-79 binding

We then analyzed the binding of HQL-79 to rat H-PGDS and its $Tyr^{8}Phe$, $Arg^{14}Glu$, $Trp^{104}Ile$, $Lys^{112}Glu$, $Cys^{156}Leu$, and $Lys^{198}Glu$ mutants by SPR analysis (**Fig. 22A**). The $Tyr^{8}Phe$ mutant showed an HQL-79-binding curve with a K_d of 0.7 μM, almost identical to that of the wild-type enzyme. Similar to the wild-type enzyme, in the absence of $MgCl_2$ the $Tyr^{8}Phe$ mutant showed a 5-fold decrease in binding affinity for HQL-79 without a change in the

maximum binding capacity. In the absence of GSH, the total binding capacity of the mutant decreased to about 50%, and the K_d value increased to 22 μM in the presence or absence of $MgCl_2$. These results indicate that the Tyr8 residue was not essential for the HQL-79-binding (27).

The $Arg^{14}Glu$ mutant gave a binding curve quite different from those curves of the wild type and other mutant enzymes (**Fig. 22B**), showing a remarkably decreased affinity for HQL-79 with a K_d of 20 μM in the presence of 2 mM $MgCl_2$ and 2 mM GSH. Although the HQL-79-binding was not saturated up to 100 μM, the maximum soluble concentration of HQL-79 in the assay buffer, the calculated maximum binding capacity was almost the same as those capacities of the wild type and Tyr^8Phe mutant enzymes. In the absence of $MgCl_2$ and in the presence of 2 mM GSH, the K_d was slightly decreased to 22 μM, but the calculated maximum binding capacity remained unchanged. In the absence of GSH, the HQL-79 binding was decreased to half of that in the presence of GSH, and the K_d value was calculated to be 48 and 47 μM with and without 2 mM $MgCl_2$, respectively. These results suggest that Arg14 was important for the Mg^{2+}-mediated increase in the binding affinity of H-PGDS for HQL-79 by increasing the affinity for GSH, as previously suggested from the kinetic analysis.

The $Trp^{104}Ile$, $Lys^{112}Glu$, and $Lys^{198}Glu$ mutants showed HQL-79-binding curves similar to each other, with a decrease in the maximum binding capacity to 26, 48 and 64%, respectively, of that of the wild type enzyme and a 3 to 5-fold

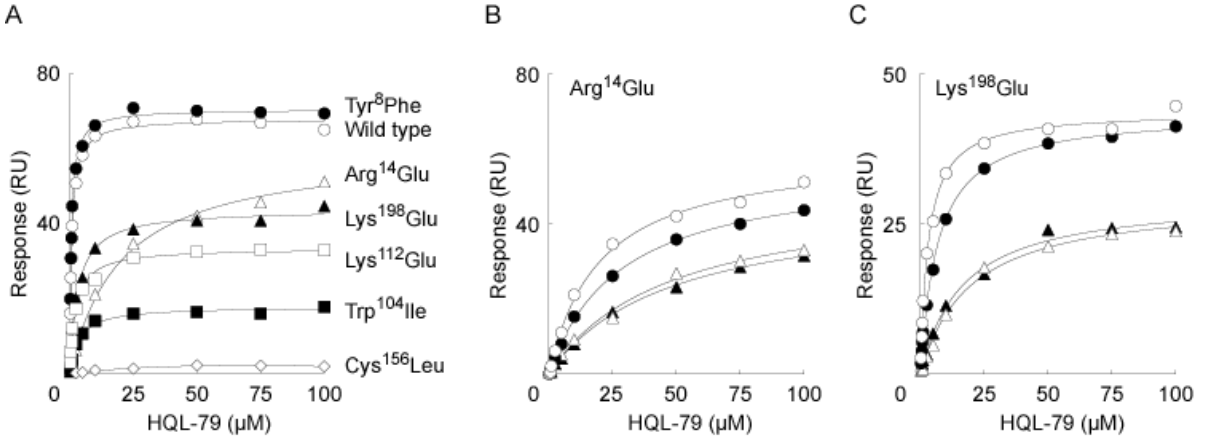

Figure 22. Effects of the mutations on HQL-79-binding (27). **A.** Dose-response curves of HQL-79 binding to immobilized rat H-PGDS and its mutants Tyr^8Phe, $Arg^{14}Glu$, $Trp^{104}Ile$, $Lys^{112}Glu$, $Cys^{156}Leu$, and $Lys^{198}Glu$ in the presence of 2 mM $MgCl_2$ and 2 mM GSH. **B. C.** Dose response curves of HQL-79 binding to immobilized rat $Arg^{14}Glu$ mutant (B), and the $Lys^{198}Glu$ mutant (C) in the absence or the presence of 2 mM $MgCl_2$ and 2 mM GSH. Open circles, 2 mM $MgCl_2$ and 2 mM GSH; closed circles, (-) $MgCl_2$ and 2 mM GSH; open triangles, 2 mM $MgCl_2$ and (-) GSH; closed triangles, (-) $MgCl_2$ and (-) GSH.

increase in the K_d value (3.6, 2.3, and 3.1 μM, respectively) in the presence of 2 mM $MgCl_2$ and 2 mM GSH. In the absence of $MgCl_2$, these mutants showed an approx. 5-fold increase in their K_d values for HQL-79 without a change in their maximum binding capacities. In the absence of GSH, their maximum binding capacities decreased to half of those in the presence of GSH; and their K_d values for HQL-79 decreased to about 16-19 μM. Typical results obtained with the $Lys^{198}Glu$ mutant are shown in **Fig. 22C**. These results suggest that the Trp104, Lys112, and Lys198 residues are important for maintaining the HQL-binding pocket.

The $Cys^{156}Leu$ mutant lost almost completely its HQL-binding activity (**Fig. 22A**), indicating that the HQL-binding pocket was fatally damaged by this mutation; although this mutant showed about 50% of the GST activity of the wild type enzyme.

6) Drug designing based on the HQL-79 binding

The crystal structure of the H-PGDS·HQL-79 complex suggests the possible strategy for drug designing. As the tetrazol ring of HQL-79 was located at the entrance of pocket 3 and did not directly interact with the positively charged amino acid cluster in pocket 3, one promising modification of HQL-79 would be the elongation of the side chain of the tetrazol group to provide a better interaction of it with these positively charged residues. Since the phenyl group of the diphenyl group of HQL-79 almost completely filled pocket 2, only minor modification with a small-sized group would be possible for this phenyl group. On the other hand, the other phenyl group of HQL-79 penetrated into the ceiling of pocket 1, resulting in the rotation of the indole ring of Trp104 and the twisting of loop7. Therefore, derivatization would be more acceptable for the phenyl group of HQL-79 within pocket 1 than for that in pocket 2. The development of novel H-PGDS inhibitors with increased selectivity and inhibitory potency is now being extensively pursued by our group and others, based on the crystal structure of the H-PGDS/HQL-79 complex (**Fig. 17A** and **B**).

Pathological involvement of H-PGDS in allergic inflammation, neuroinflammation, and muscular dystrophy

Orally administered HQL-79 (30 mg/kg body weight) inhibited antigen-induced production of PGD_2, without affecting the production of PGE_2 and $PGF_{2\alpha}$, and ameliorated airway inflammation in wild-type and human H-PGDS-over-expressing mice (**Fig. 23**). PGD_2 produced by H-PGDS in human mast cells and Th2 cells accelerates allergy and inflammation responses by

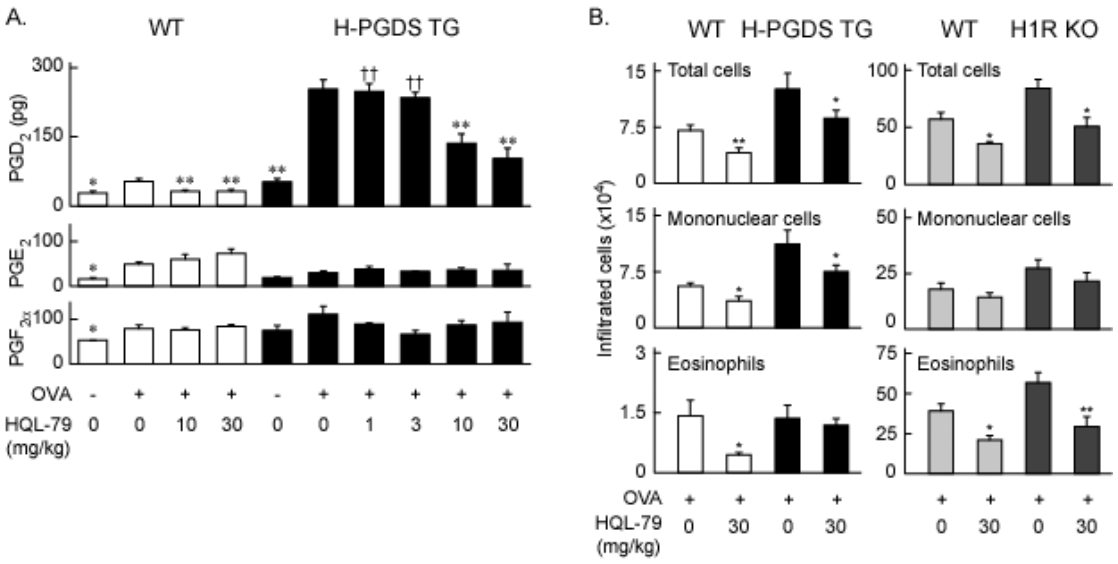

Figure 23. Inhibition of antigen-induced production of PGD_2 and airway inflammation in wild-type and human H-PGDS-over-expressing mice by oral administration of HQL-79 (27). A. Selective inhibition of the PGD_2 release into bronchoalveolar lavage fluid of ovalbumin-sensitized mice by HQL-79. HQL-79 †† $p<0.01$ as compared with 30 mg/kg of HQL-79 (Dunnett's test). B. Suppression by HQL-79 of leukocyte infiltration in WT and H-PGDS-TG mice (left panels) and WT and H1R KO mice (right panels). *$p<0.05$, **$p<0.01$ (Student's *t*-test).

stimulating DP_2 receptors on Th2 cells in an autocrine manner, and DP_1 and DP_2 receptors on those other cells in a paracrine manner (27). Therefore, human H-PGDS is a promising target for designing anti-allergy and anti-inflammation drugs.

Recently, we and many other research groups reported that PGD_2 produced by H-PGDS is involved in a variety of allergic and non-allergic disorders. For example, H-PGDS is expressed in mast cells that accumulate in the nasal mucosa of patients with polyposis (S.H. and Y.U.; unpublished results) in infiltrates of mast cells, eosinophils, macrophages, and lymphocytes in the nasal mucosa of patients with allergic rhinitis (39) (45); in necrotic muscle fibers of patients with Duchenne's muscular dystrophy (**Fig. 24**) or polymyositis (41); in microglial cells around the region of demyelination in twitcher mice, an animal model of human Krabbe's disease (40); and in rat and mouse brains after stab-wounding or traumatic brain injury (K.A., Y.U.; unpublished results).

Therefore, H-PGDS inhibitors would also be predicted to suppress the progression of those diseases. In fact, we have already confirmed that genetic depletion of H-PGDS or HQL-79 administration suppressed the astrogliosis and neuroinflammation in the tw itcher mouse (40) (**Fig. 25**). Being not only effective against this genetic demyelinating disease, HQL-79 also reduced the area of injury and the astrogliosis in a stab-wound model of brain injury (K.A., Y.U., unpublished result). Furthermore we found that HQL-79 administration suppressed the expansion of muscular necrosis in *mdx* mice, an

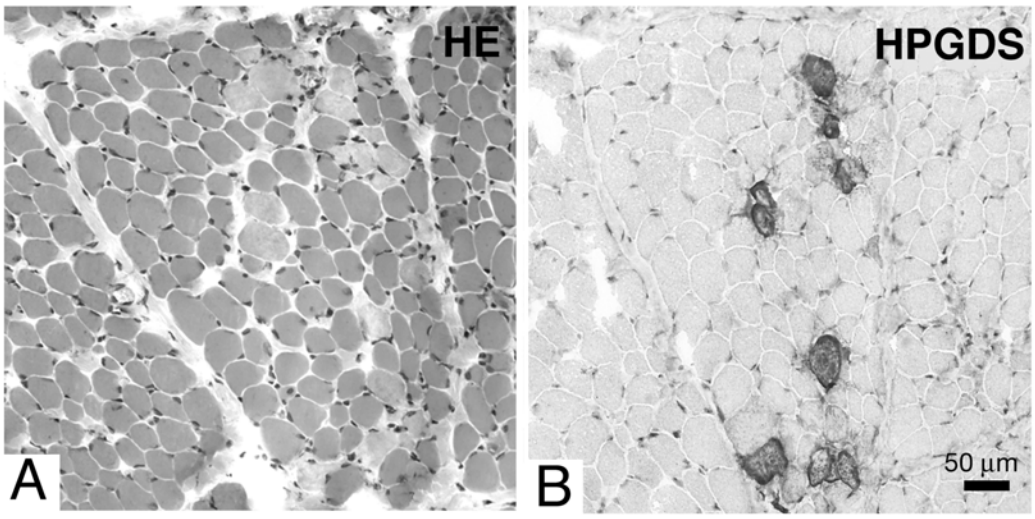

Figure 24. H-PGDS expression in necrotic muscle fibers of Duchenne's muscular dystrophy (41).

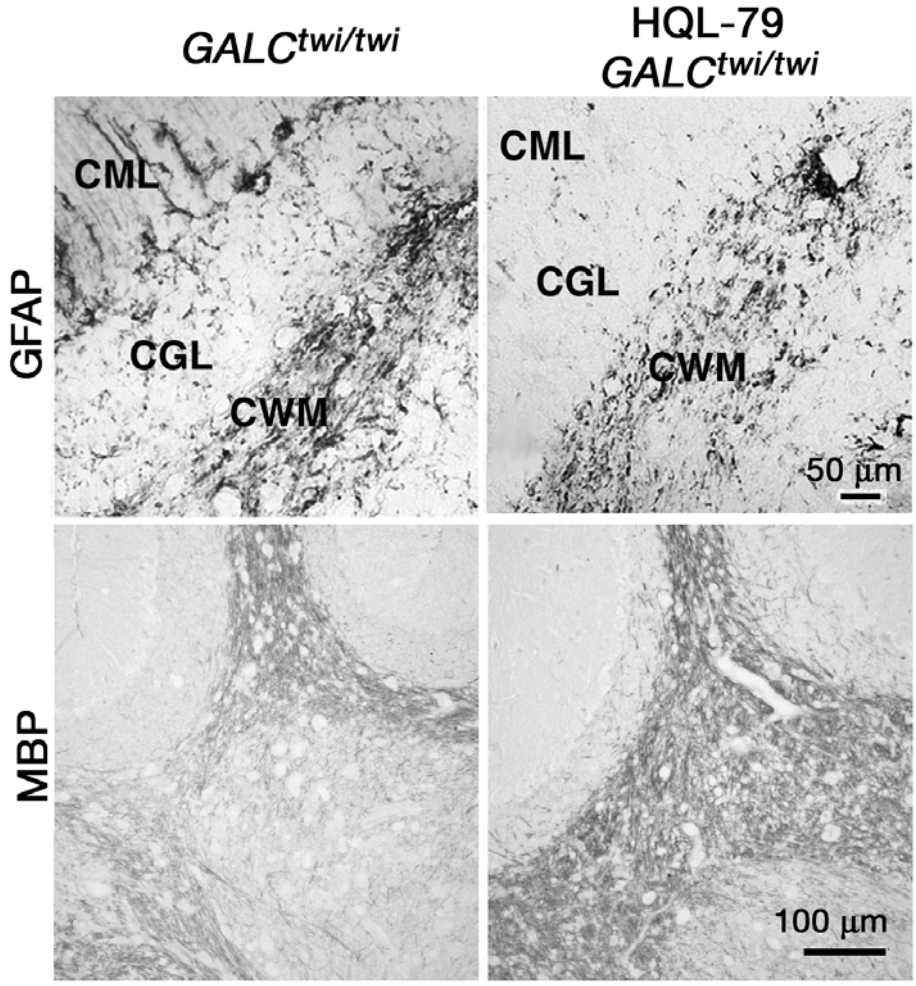

Figure 25. Gliosis and demyelination were suppressed by HQL-79 in *GALC*$^{twi/twi}$ (40). CML, cerebellar molecular layer; CGL, cerebellar granular layer; CWM, cerebellar white matter; GFAP, glial fibrillary acidic protein; MBP, myelin basic protein.

animal model of Duchenne's muscular dystrophy (I.M., Y.U.; unpublished result). These results indicate that blockade of H-PGDS/PGD_2/DP signaling would be a hopefully strongly effective therapy for neuroinflammation and muscular dystrophy. HQL-79 appears to be an excellent lead compound for the development of novel H-PGDS inhibitors that promise to be new-concept drugs against a variety of allergic and non-allergic diseases.

Acknowledgements

We also thank F. Arisaka (Tokyo Institute of Technology) for urtracentrifugation analysis, M.Taniike (Osaka University), K. Suzuki (University of North Carolina at Chapel Hill) for providing twithcher mice, M. Murakami (Tokyo Metropolitan Institute of Medical Science) for providing HEK-293 cells stably transfected with human L-PGDS and COX-1 cDNAs, Y. Kanaoka, Y. Satoh, N. Uodome, K. Fujimori, D. Irikura and I. Okazaki (Osaka Bioscience Institute) for cDNA cloning, data collection with mdx mice, assistance in enzyme assays, genetic analysis, crystallization, and SPR analysis, respectively, H. Ago (RIKEN) for the first structure of H-PGDS from rat, and H. Matsumura, N. Okazaki, H. Shishitani, S. Kinugasa, N. Katsuyama, and Y. Kado (Osaka University) for structure analyses of human H-PGDS. This work was supported by the Applied Research Pilot Project for the Industrial Use of Space promoted by Japan Science and Technology Agency and Japan Space Utilization Promotion Center (to Y.U. and T.I), a grant from Japan Foundation for Applied Enzymology (to Y.U.), the Program for Promotion of Fundamental Studies in Health Sciences of the National Institute of Biomedical Innovation (NIBIO), a Grant-in –Aid for Scientific Research of MEXT (17659022 to K.A.), the National Project on Protein Structural and Functional Analyses (to T.I.), The Mitsubishi Foundation (to Y. U.).

References

1. Urade, Y., Ujihara, M., Horiguchi, Y., Igarashi, M., Nagata, A., Ikai, K., and Hayaishi, O. (1990) *J Biol Chem* **265**, 371-375
2. Tanaka, K., Ogawa, K., Sugamura, K., Nakamura, M., Takano, S., and Nagata, K. (2000) *J Immunol* **164**, 2277-2280
3. Urade, Y., and Hayaishi, O. (2000) *Vitam Horm* **58**, 89-120
4. Mohri, I., Eguchi, N., Suzuki, K., Urade, Y., and Taniike, M. (2003) *Glia* **42**, 263-274
5. Urade, Y., Kitahama, K., Ohishi, H., Kaneko, T., Mizuno, N., and Hayaishi, O. (1993) *Proc Natl Acad Sci U S A* **90**, 9070-9074
6. Beuckmann, C. T., Lazarus, M., Gerashchenko, D., Mizoguchi, A., Nomura, S., Mohri, I., Uesugi, A., Kaneko, T., Mizuno, N., Hayaishi, O., and Urade, Y. (2000) *J Comp Neurol* **428**, 62-78
7. Matsuoka, T., Hirata, M., Tanaka, H., Takahashi, Y., Murata, T., Kabashima, K., Sugimoto, Y., Kobayashi, T., Ushikubi, F., Aze, Y., Eguchi, N., Urade, Y.,

Yoshida, N., Kimura, K., Mizoguchi, A., Honda, Y., Nagai, H., and Narumiya, S. (2000) *Science* **287**, 2013-2017
8. Nagata, K., and Hirai, H. (2003) *Prostaglandins Leukot Essent Fatty Acids* **69**, 169-177
9. Chevalier, E., Stock, J., Fisher, T., Dupont, M., Fric, M., Fargeau, H., Leport, M., Soler, S., Fabien, S., Pruniaux, M. P., Fink, M., Bertrand, C. P., McNeish, J., and Li, B. (2005) *J Immunol* **175**, 2056-2060
10. Fujitani, Y., Kanaoka, Y., Aritake, K., Uodome, N., Okazaki-Hatake, K., and Urade, Y. (2002) *J Immunol* 168, 443-449
11. Smith, W. L., Marnett, L. J., and DeWitt, D. L. (1991) *Pharmacol Ther* **49**, 153-179
12. Fitzpatrick, F. A., and Wynalda, M. A. (1983*) J Biol Chem* 258, 11713-11718
13. Forman, B. M., Tontonoz, P., Chen, J., Brun, R. P., Spiegelman, B. M., and Evans, R. M. (1995) *Cell* **83**, 803-812
14. Kliewer, S. A., Lenhard, J. M., Willson, T. M., Patel, I., Morris, D. C., and Lehmann, J. M. (1995) *Cell* **83**, 813-819
15. Hirata, Y., Hayashi, H., Ito, S., Kikawa, Y., Ishibashi, M., Sudo, M., Miyazaki, H., Fukushima, M., Narumiya, S., and Hayaishi, O. (1988) *J Biol Chem* **263**, 16619-16625
16. Bell-Parikh, L. C., Ide, T., Lawson, J. A., McNamara, P., Reilly, M., and FitzGerald, G. A. (2003) *J Clin Invest* **112**, 945-955
17. Powell, W. S. (2003) *J Clin Invest* **112**, 828-830
18. Christ-Hazelhof, E., and Nugteren, D. H. (1979) *Biochim Biophys Acta* **572**, 43-51
19. Urade, Y., Fujimoto, N., and Hayaishi, O. (1985) *J Biol Chem* **260**, 12410-12415
20. Urade, Y., and Hayaishi, O. (2000) *Biochim Biophys Acta* **1482**, 259-271
21. Urade, Y., Eguchi, N., and Hayaishi, O. (2006) Lipocalins, Landes Bioscience / Eurekah.com, Chapter 9, 99-109 (ed. by Åkerström, B., Flower, D., Salier, J.P.), 99-109
22. Shimizu, T., Yamamoto, S., and Hayaishi, O. (1979) *J Biol Chem* **254**, 5222-5228
23. Urade, Y., Fujimoto, N., Ujihara, M., and Hayaishi, O. (1987) *J Biol Chem* **262**, 3820-3825
24. Toh, H., Kubodera, H., Nakajima, N., Sekiya, T., Eguchi, N., Tanaka, T., Urade, Y., and Hayaishi, O. (1996) *Protein Eng* 12, 1067-1082
25. Urade, Y., and Eguchi, N. (2002) *Prostaglandins Other Lipid Mediat* **68-69**, 375-382
26. Inoue, T., Irikura, D., Okazaki, N., Kinugasa, S., Matsumura, H., Uodome, N., Yamamoto, M., Kumasaka, T., Miyano, M., Kai, Y., and Urade, Y. (2003) *Nat Struct Biol* **10**, 291-296
27. Aritake, K., Kado, Y., Inoue, T., Miyano, M., and Urade, Y. (2006) *J Biol Chem* **281**, 15277-15286
28. Matsushita, N., Aritake, K., Takada, A., Hizue, M., Hayashi, K., Mitsui, K., Hayashi, M., Hirotsu, I., Kimura, Y., Tani, T., and Nakajima, H. (1998) *Jpn J Pharmacol* **78**, 11-22
29. Editorial. (2003) *Nat Struct Biol* **10**, 233
30. Kunikata, T., Yamane, H., Segi, E., Matsuoka, T., Sugimoto, Y., Tanaka, S., Tanaka, H., Nagai, H., Ichikawa, A., and Narumiya, S. (2005) *Nat Immunol* **6**, 524-531
31. Taniike, M., Mohri, I., Eguchi, N., Beuckmann, C. T., Suzuki, K., and Urade, Y. (2002) *J Neurosci* **22**, 4885-4896

32. Ujihara, M., Urade, Y., Eguchi, N., Hayashi, H., Ikai, K., and Hayaishi, O. (1988) *Arch Biochem Biophys* **260**, 521-531
33. Kanaoka, Y., Ago, H., Inagaki, E., Nanayama, T., Miyano, M., Kikuno, R., Fujii, Y., Eguchi, N., Toh, H., Urade, Y., and Hayaishi, O. (1997) *Cell* **90**, 1085-1095
34. Kanaoka, Y., Fujimori, K., Kikuno, R., Sakaguchi, Y., Urade, Y., and Hayaishi, O. (2000) *Eur J Biochem* **267**, 3315-3322
35. Thomson, A. M., Meyer, D. J., and Hayes, J. D. (1998) *Biochem J* **333 (Pt 2)**, 317-325
36. Ujihara, M., Horiguchi, Y., Ikai, K., and Urade, Y. (1988) *J Invest Dermatol* **90**, 448-451
37. Urade, Y., Ujihara, M., Horiguchi, Y., Ikai, K., and Hayaishi, O. (1989) *J Immunol* **143**, 2982-2989
38. Mahmud, I., Ueda, N., Yamaguchi, H., Yamashita, R., Yamamoto, S., Kanaoka, Y., Urade, Y., and Hayaishi, O. (1997) *J Biol Chem* **272**, 28263-28266
39. Okano, M., Fujiwara, T., Sugata, Y., Gotoh, D., Masaoka, Y., Sogo, M., Tanimoto, W., Yamamoto, M., Matsumoto, R., Eguchi, N., Kiniwa, M., Umit Isik, A., Urade, Y., and Nshizaki, K. (2006) *American J. Rhinology* **20**, 342-348
40. Mohri, I., Taniike, M., Taniguchi, H., Kanekiyo, T., Aritake, K., Inui, T., Fukumoto, N., Eguchi, N., Kushi, A., Sasai, H., Kanaoka, Y., Ozono, K., Narumiya, S., Suzuki, K., and Urade, Y. (2006) *J Neurosci* **26**, 4383-4393
41. Okinaga, T., Mohri, I., Fujimura, H., Imai, K., Ono, J., Urade, Y., and Taniike, M. (2002) *Acta Neuropathol (Berl)* **104**, 377-384
42. Ujihara, M., Tsuchida, S., Satoh, K., Sato, K., and Urade, Y. (1988) *Arch Biochem Biophys* **264**, 428-437
43. Beuckmann, C. T., Fujimori, K., Urade, Y., and Hayaishi, O. (2000) *Neurochem Res* **25**, 733-738
44. Pinzar, E., Miyano, M., Kanaoka, Y., Urade, Y., and Hayaishi, O. (2000) *J Biol Chem* **275**, 31239-31244
45. Kanaoka, Y., Ago, H., Inagaki, E., Nanayama, T., Miyano, M., Kikuno, R., Fujii, Y., Eguchi, N., Toh, H., Urade, Y., and Hayaishi, O. (1999) *Erratum in Cell* **96**, 449
46. Okano, M., Fujiwara, T., Yamamoto, M., Sugata, Y., Matsumoto, R., Fukushima, K., Yoshino, T., Shimizu, K., Eguchi, N., Kiniwa, M., Urade, Y., and Nishizaki, K. (2006) *Clin Exp Allergy* **36**, 1028-1038